Cell Metabolism
Article

Activation of Calcium/Calmodulin-Dependent Protein Kinase II in Obesity Mediates Suppression of Hepatic Insulin Signaling

Lale Ozcan,[1,*] Jane Cristina de Souza,[1] Alp Avi Harari,[1] Johannes Backs,[4,5] Eric N. Olson,[6] and Ira Tabas[1,2,3,*]
[1]Department of Medicine
[2]Department of Physiology and Cellular Biophysics
[3]Department of Pathology and Cell Biology
Columbia University, New York, NY 10032, USA
[4]Laboratory for Cardiac Epigenetics, Department of Cardiology, Heidelberg University, Heidelberg 69120, Germany
[5]DZHK-German Centre for Cardiovascular Research, Heidelberg 69120, Germany
[6]Department of Molecular Biology, University of Texas Southwestern Medical Center, Dallas, TX 75390, USA
*Correspondence: lo2192@columbia.edu (L.O.), iat1@columbia.edu (I.T.)
http://dx.doi.org/10.1016/j.cmet.2013.10.011

SUMMARY

A hallmark of obesity is selective suppression of hepatic insulin signaling ("insulin resistance"), but critical gaps remain in our understanding of the molecular mechanisms. We now report a major role for hepatic CaMKII, a calcium-responsive kinase that is activated in obesity. Genetic targeting of hepatic CaMKII, its downstream mediator p38, or the p38 substrate and stabilizer MK2 enhances insulin-induced p-Akt in palmitate-treated hepatocytes and obese mouse liver, leading to metabolic improvement. The mechanism of improvement begins with induction of ATF6 and the ATF6 target $p58^{IPK}$, a chaperone that suppresses the PERK—p-eIF2α—ATF4 branch of the UPR. The result is a decrease in the ATF4 target TRB3, an inhibitor of insulin-induced p-Akt, leading to enhanced activation of Akt and its downstream metabolic mediators. These findings increase our understanding of the molecular mechanisms linking obesity to selective insulin resistance and suggest new therapeutic targets for type 2 diabetes and metabolic syndrome.

INTRODUCTION

Obesity is the leading cause of insulin resistance, metabolic syndrome, and type 2 diabetes (T2D), but therapeutic options are limited due to critical gaps in our knowledge of molecular mechanisms linking obesity with the metabolic disturbances of insulin resistance and T2D (Samuel and Shulman, 2012). A key factor in T2D is an inappropriate increase in hepatic glucose production (HGP), which results from selective hepatic insulin resistance together with impaired suppression of glucagon signaling (Lin and Accili, 2011). In addition to elevated HGP, selective insulin resistance contributes to other critical maladies associated with T2D, including cardiovascular disease, the leading cause of death in these patients (Bornfeldt and Tabas, 2011; Leavens and Birnbaum, 2011).

We recently elucidated a pathway through which glucagon stimulates HGP in fasting and in obesity, and in obesity this pathway contributes to hyperglycemia (Ozcan et al., 2012; Wang et al., 2012). The pathway is triggered downstream of the glucagon receptor by PKA-mediated activation of the endoplasmic reticulum (ER) calcium release channel, inositol 1,4,5-triphosphate receptor (IP3R). Channel opening, which is also promoted by a glucagon receptor-phospholipase C pathway that generates IP3, results in release of calcium from ER stores, which then activates the cytoplasmic calcium-sensitive kinase, calcium/calmodulin dependent-protein kinase II (CaMKII). CaMKII then activates the MAPK p38α, which phosphorylates FoxO1 in a manner that promotes FoxO1 nuclear translocation. Nuclear FoxO1 induces target genes that are rate limiting for glycogenolysis and gluconeogenesis, notably *G6pc* and *Pck1*. This CaMKII-FoxO1 pathway is complemented by the activation of the calcium-sensitive phosphatase calcineurin, which promotes CRTC2-mediated induction of the FoxO1 transcriptional partner, PGC1α (Wang et al., 2012). Moreover, recent studies have shown that calcium transport back into the ER, mediated by sarcoplasmic/endoplasmic reticulum calcium ATPase (SERCA), is dysfunctional in obesity (Fu et al., 2011; Park et al., 2010), which could contribute to both the amplitude and the duration of the pathological calcium response. Collectively, these data point to the importance of intracellular calcium metabolism and CaMKII in enhanced HGP in obesity. However, a critical remaining question in this area was whether CaMKII plays a role in the other major pathological process in obesity and T2D, namely selective insulin resistance.

Defective insulin signaling is a major feature of selective hepatic insulin resistance in obesity (Brown and Goldstein, 2008; Könner and Brüning, 2012). In normal physiology, insulin stimulates insulin autophosphorylation of the insulin receptor (IR), which promotes to Tyr-phosphorylation of insulin receptor substrates 1 and 2 (IRS-1/2). Through a series of downstream processes involving lipid mediators and protein kinases, p-IRS-1/2 leads to Ser/Thr-phosphorylation and activation of

Akt (also known as protein kinase B) (Saltiel and Kahn, 2001). Akt-induced phosphorylation of a number of substrates is critically involved in promoting the anabolic effects of insulin on glucose and lipid metabolism. In obesity and T2D, insulin-induced phosphorylation of Akt is defective, which disables the pathway that normally suppresses HGP (Lin and Accili, 2011). In theory, defective Akt phosphorylation could occur at the level of the IR, IRS1/2, signal transducers downstream of IRS-1/2, or Akt phosphorylation itself. Studies in obese mouse models have shown evidence for defects in each of these steps, depending on the model used and the focus of the investigation, and there is also evidence for defects in insulin-induced p-Akt in humans with T2D (Brozinick et al., 2003; Krook et al., 1998; Saad et al., 1992). Moreover, the resulting hyperinsulinemia excessively stimulates nonresistant insulin pathways that mediate hepatic lipid synthesis and storage (Brown and Goldstein, 2008) and is associated with other maladies associated with T2D, such as atherosclerosis (Bornfeldt and Tabas, 2011; Leavens and Birnbaum, 2011). Because perturbation of proximal insulin signaling is one of the earliest hallmarks of T2D and is responsible for the most important complications of obesity and T2D, identification of the molecular mechanisms responsible for this defect has the potential to aid in the development of new and more specific antidiabetic drugs.

In this report, we identify a CaMKII/p38-mediated pathway that plays a critical role in obesity-associated insulin resistance in the liver. This pathway is independent of the aforementioned CaMKII/p38-FoxO1 pathway involved in HGP in obesity. We provide evidence that obesity-activated CaMKII/p38 suppresses insulin-induced Akt phosphorylation by activating the ER stress effector ATF4, which in turn induces the Akt inhibitor, TRB3. Thus, an integrated, calcium-based paradigm in hepatocytes involved in the two cardinal features of T2D, hyperglycemia and defective insulin signaling, is beginning to emerge, providing new potential therapeutic targets.

RESULTS

Inhibition of Liver CaMKII, p38α, or MAPKAPK2 in Obese Mice Lowers Plasma Insulin and Improves the Response to Glucose Challenge

We first evaluated the role of CaMKII on plasma insulin levels and response to glucose in three models of obese mice. In the first model, liver CaMKII in *ob/ob* mice was inhibited through the use of an adenoviral vector expressing K43A-CaMKII (Pfleiderer et al., 2004), which is a kinase-inactive, dominant-negative (DN) form that has been shown to inhibit hepatic CaMKII (Ozcan et al., 2012). We showed previously that adeno-K43A-CaMKII treatment of *ob/ob* mice, as compared with *ob/ob* mice treated with adeno-LacZ control vector, lowered blood glucose (Ozcan et al., 2012). This effect occurred in the absence of any change in body weight (44.8 ± 1.9 g versus 43.5 ± 1.6 g), food intake (5.3 ± 0.3 g versus 5 ± 0.2 g per mouse per day), or epididymal fat pad mass (3.2 ± 0.2 g versus 3 ± 0.1 g). Moreover, K43A-CaMKII-treated mice displayed a more than 2-fold reduction in plasma insulin concentration compared with control adeno-LacZ-treated mice (Figure 1A), consistent with an increase in insulin sensitivity. In support of this conclusion, adeno-K43A-CaMKII-treated *ob/ob* mice exhibited significantly lower glucose levels during glucose and insulin tolerance tests (Figures 1B and 1C).

In the second model, liver CaMKIIγ, which is the CaMKII isoform in hepatocytes, was deleted in diet-induced obese (DIO) mice by injecting DIO *Camk2g*$^{fl/fl}$ mice with adeno-associated virus-8 encoding Cre recombinase driven by the hepatocyte-specific thyroxin-binding globulin promoter (AAV8-TBG-Cre) (Sun et al., 2012). This treatment successfully silenced *Camk2g* in the hepatocytes (Figure 1D) without changing body weight (44.6 ± 2.29 g versus 43 ± 0.7 g), food intake (3.13 ± 0.17 g versus 2.92 ± 0.19 g per mouse per day), or epididymal fat pad mass (2.4 ± 0.14 g versus 2.24 ± 0.07 g). Consistent with the *ob/ob* data, DIO mice that lack hepatocyte CaMKIIγ had lower fasting insulin levels (Figure 1E), lower blood glucose levels (Figure 1F), and an improved blood glucose response to glucose challenge (Figure 1G). Similar results were found using a third model, in which holo-CaMKIIγ KO (*Camk2g*$^{-/-}$) mice were placed on the high fat diet (see Figures S1A and S1B available online).

Consistent with an improvement in insulin resistance, targeting hepatocyte CaMKIIγ in obese mice (AAV8-TBG-Cre) led to a decrease in hepatic steatosis (Figure S1C); hepatocyte TG content was also decreased in the Cre-treated mice (79.13 ± 7.21 versus 59.6 ± 7.27 mg per g liver). The decrease in hepatic steatosis was not due to an increase in triglyceride secretion, as the Cre-treated mice had a decrease in plasma triglyceride levels (266.78 ± 28.08 versus 193.34 ± 13.01 mg per dl). These combined data suggest that hepatic CaMKIIγ plays a central role in the manifestations of obesity-induced insulin resistance.

Hepatic p38 activation has been implicated in insulin resistance in obese mice (Hemi et al., 2011), but the upstream and downstream mechanisms remain incompletely understood. We have previously shown that CaMKII regulates p38α MAPK activity in hepatocytes (Ozcan et al., 2012), and so we explored the possibility that p38 might also function as a downstream mediator of CaMKII in the pathogenesis of insulin resistance. To this end, the gene encoding p38α (*Mapk14*) was silenced in hepatocytes by injecting DIO *Mapk14*$^{fl/fl}$ mice with AAV-TBG-Cre, which led to more than 90% silencing of p38α protein levels in liver (below) without affecting body weight (41 ± 2.36 g versus 39 ± 1.04 g), food intake (2.62 ± 0.09 g versus 2.24 ± 0.06 g per mouse per day), or epididymal fat pad mass (1.92 ± 0.15 g versus 1.83 ± 0.14 g). Compared with control mice (AAV-TBG-LacZ), mice deficient in hepatocyte p38α had lower fasting blood glucose (Figure 2A), lower plasma insulin levels (Figure 2B), improved blood glucose response to glucose challenge, and enhanced glucose disposal upon insulin stimulation (Figures 2C and 2D).

MAPK-activating protein kinase 2 (MK2) is a well-characterized downstream effector of p38 (Freshney et al., 1994; Rouse et al., 1994). Moreover, activated MK2 forms a tight complex with p38α and thus reciprocally stabilizes p38α (Gaestel, 2006). To investigate the role of MK2, *ob/ob* mice were injected i.v. with adenovirus encoding MK2 with a mutation in its p38 phosphorylation site (T222A), which acts as a DN form of the enzyme (Streicher et al., 2010). This treatment resulted in lowering of blood glucose (Figure 2E) and plasma insulin levels (Figure 2F) and a marked improvement in glucose tolerance (Figure 2G), without changing body weight (49.4 ± 2.01 g versus

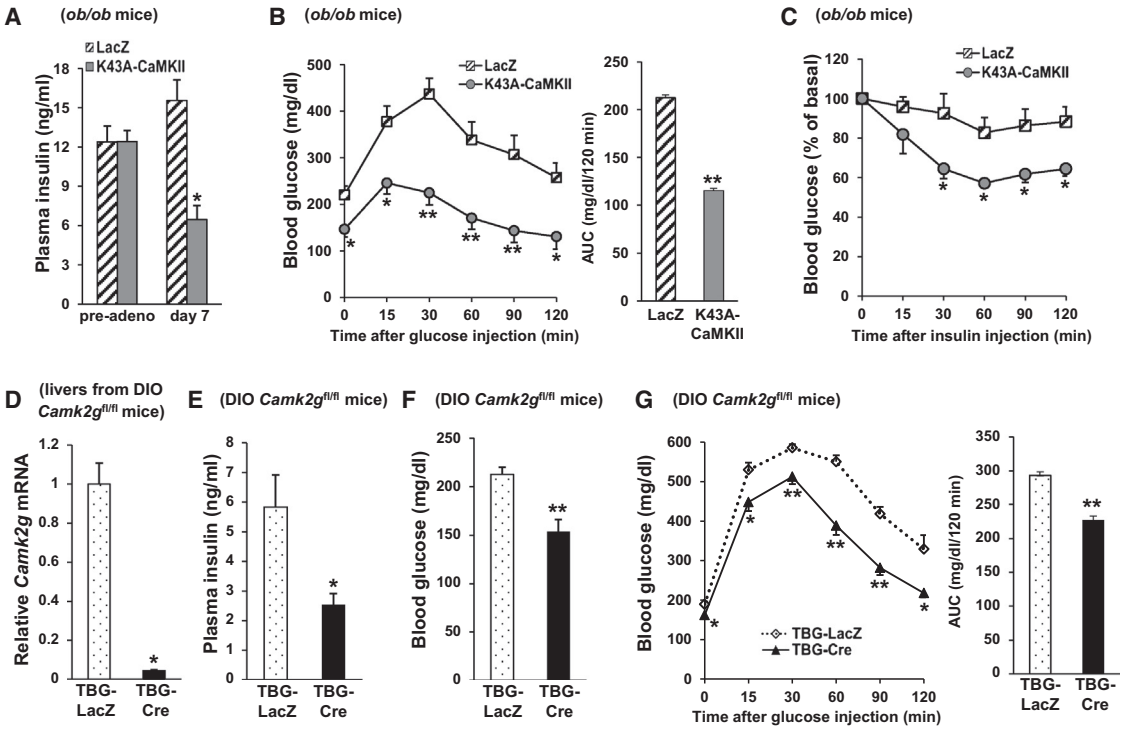

Figure 1. Inhibition or Deletion of Liver CaMKIIγ Lowers Plasma Insulin and Improves Response to Glucose and Insulin Challenge in Obese Mice

(A) Nine-week-old *ob/ob* mice were fasted for 6 hr, assayed for plasma insulin ("pre-adeno"), and then injected with adeno-LacZ (n = 6) or adeno-K43A-CaMKII (n = 6). Seven days later, after a 6 hr fast, the mice were assayed again for plasma insulin ("day 7") (*p < 0.05, **p < 0.01; mean ± SEM).

(B) Glucose tolerance tests were performed after overnight fasting (*p < 0.05, **p < 0.01; mean ± SEM). Area under the curve (AUC) is quantified in the right panel (**p < 0.01; mean ± SEM).

(C) Insulin tolerance tests were performed after 6 hr fasting (*p < 0.05; mean ± SEM).

(D–G) Liver *CaMKIIγ* mRNA, fasting plasma insulin, fasting blood glucose, and blood glucose after glucose challenge in DIO *Camk2g*$^{fl/fl}$ mice after treatment with adeno-associated virus (AAV) containing either hepatocyte-specific TBG-Cre recombinase (TBG-Cre) (n = 5) or the control vector (TBG-LacZ) (n = 5) (*p < 0.05, **p < 0.01; mean ± SEM). AUC for the glucose tolerance test is quantified in the right panel (**p < 0.01; mean ± SEM).

See also Figure S1.

51.4 ± 0.67 g) or food intake (5.37 ± 0.44 g versus 5.52 ± 0.23 g per mouse per day). Thus, liver p38α and MK2, like CaMKII, play an important role in the development of hyperglycemia and hyperinsulinemia in obese mice and the response of these mice to exogenous glucose.

Deletion or Inhibition of CaMKII, p38α, or MK2 Improves Insulin-Induced Akt Phosphorylation in Obese Mice

In view of the above data, we focused our attention on hepatocyte insulin signaling, where defects contribute to insulin resistance in obesity (Brown and Goldstein, 2008). As a measure of hepatic insulin signaling, we assayed pSer^{473}-Akt in the livers of mice injected with insulin through the portal vein. The data show a significant increase in insulin-induced p-Akt in the livers of *Camk2g*$^{-/-}$ DIO mice compared with WT DIO mice (Figure 3A, top two blots). Improvements in Akt phosphorylation are often associated with increased tyrosine phosphorylation of IR and/or IRS-1/2. However, in the case of DIO CaMKII KO mice, phosphorylation of neither IR (data not shown) nor IRS-1 was increased (Figure 3A, bottom two blots). Similar results were found in DIO *Camk2g*$^{fl/fl}$ mice injected with AAV-TBG-Cre and in *ob/ob* mice treated with DN adeno-K43A-CaMKII: insulin-induced phosphorylation of Akt was increased, but phosphorylation of IR and IRS-1 was not (Figures 3B and S2A). Note that inhibition of CaMKII in chow-fed lean mice did not induce significant changes in p-Akt levels (Figure S2B), indicating a specific role of CaMKII in defective insulin-induced p-Akt in obese mice.

The data in Figure 2 showed that liver-directed silencing of either p38, which is a downstream target of CaMKII, or MK2, which is a substrate and stabilizer of p38, improved plasma insulin and response to glucose and insulin. To link these findings to hepatic insulin signaling, we treated DIO *Mapk14*$^{fl/fl}$ mice with AAV-TBG-Cre and then assayed insulin-induced p-Akt. As with CaMKII silencing, there was enhanced insulin-stimulated Akt phosphorylation without an increase in IR or IRS-1/2 phosphorylation (Figure 3C). Similarly, Akt activation was increased in *ob/ob* mice injected with DN adeno-T222A-MK2 (Figure S2C) without an increase in the phosphorylation of IR or IRS proteins (data not shown). These combined data indicate that CaMKII, p38α, and MK2 participate in defective insulin-p-Akt signaling in the livers of obese mice at a step to distal to IRS phosphorylation.

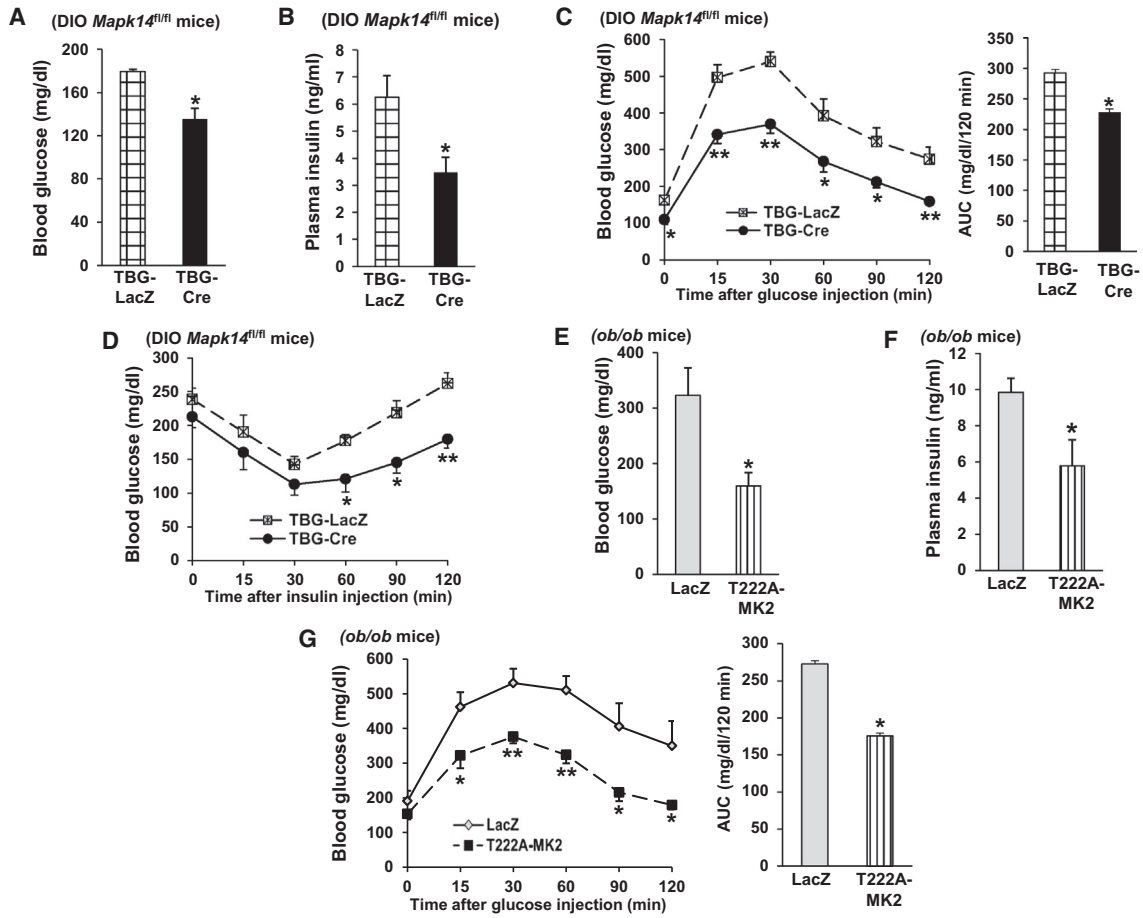

Figure 2. Inhibition or Deletion of p38α or MAPKAPK2 (MK2) Lowers Plasma Glucose and Insulin and Improves Response to Glucose and Insulin Challenge in Obese Mice

(A–D) Fasting blood glucose, plasma insulin, glucose, and insulin tolerance tests in DIO *Mapk14*$^{fl/fl}$ mice after treatment with AAV-TBG-LacZ (n = 5) or AAV-TBG-Cre (n = 5) (*p < 0.05; mean ± SEM). Area under the curve (AUC) for the glucose tolerance test is quantified in the right panel (*p < 0.05; mean ± SEM).

(E–G) Fasting blood glucose and plasma insulin; and blood glucose after glucose challenge in *ob/ob* mice administered 1 × 10^9 pfu of adeno-LacZ (n = 5) or adeno-T222A-MK2 (n = 5) (*p < 0.05, **p < 0.01; mean ± SEM). AUC for the glucose tolerance test is quantified in the right panel (*p < 0.05; mean ± SEM).

Inhibition of CaMKII or p38α Improves Insulin-Induced Akt Phosphorylation Distal to IR and IRS and in a FoxO1-Independent Manner

To further probe mechanism, we moved to a primary murine hepatocyte (HC) model in which insulin-induced Akt phosphorylation is suppressed by treatment with the saturated fatty acid palmitate (Achard and Laybutt, 2012). Using transduction with adeno-K43A-CaMKII, we first showed that this model recapitulates the improvement in insulin-induced Akt phosphorylation observed with CaMKII inhibition in vivo (Figure 4A, top three blots), whereas adeno-K43A-CaMKII transduction did not evoke any significant changes under the control, BSA-treated group. Moreover, consistent with our in vivo findings, CaMKII inhibition did not enhance Tyr-phosphorylation of IRS-1 (Figure 4A, right panel), IR, or IRS-2 (data not shown). Similar data were obtained using p38α-deficient hepatocytes in terms of p-Akt (Figure 4B, upper panel, top three blots) and p-IR and p-IRS-1 (Figure 4B, left lower panel). Consistent with improved Akt activation, insulin-stimulated phosphorylation of the downstream Akt targets, FoxO1 and GSK-3β, were also significantly improved (Figure 4B, right lower panel, bottom four blots), and glucose output was significantly inhibited (49.97 ± 2.76 versus 82.78 ± 4.66 nmol/hr/mg protein). Furthermore, in order to acquire information about the human relevance of our murine HC studies, we tested the effect of CaMKII inhibition in metabolism-qualified human HCs using the palmitate model. Consistent with our murine HC data, palmitate-induced suppression of insulin-induced p-Akt was prevented by CaMKII inhibition using adeno-K43A-CaMKII (Figure 4C).

We next examined whether a constitutively active mutant of CaMKII (CA-CaMKII) is sufficient to interfere with insulin action in the absence of palmitate. This mutant possesses an amino acid substitution, T287D, which mimics autophosphorylation at T287 and results in autonomous activity in the absence of bound calcium/calmodulin (Ozcan et al., 2012; Pfleiderer et al., 2004). The data show that CA-CaMKII resulted in a decrease in insulin-induced Akt phosphorylation without decreasing either p-IRS-1, which was actually increased, or p-IRS-2 (Figure 4D).

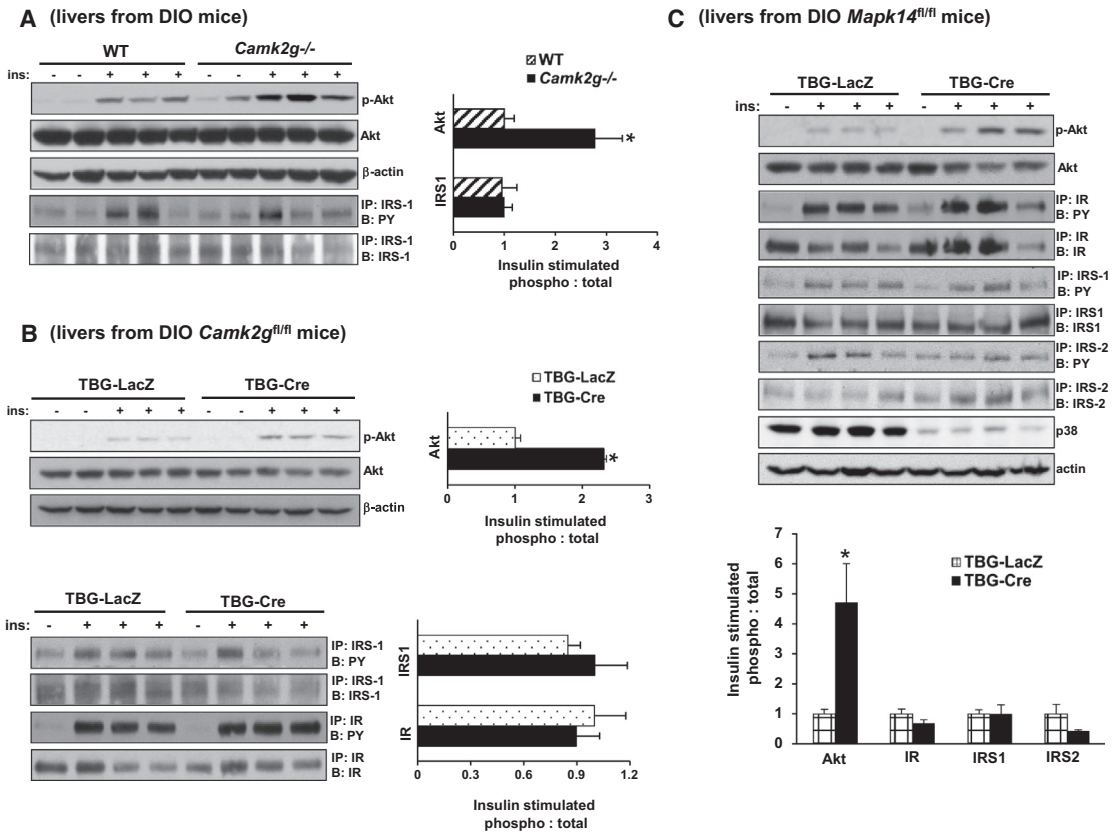

Figure 3. Deletion of CaMKII or p38α Improves Insulin-Induced Akt Phosphorylation in Obese Mice

(A) DIO *Camk2g*$^{-/-}$ or WT mice were fasted for 6 hr and then injected with 1.5 IU/kg insulin through the portal vein. Total liver extracts were then assayed for p-Akt, total Akt, and β-actin by immunoblot or immunoprecipitated (IP:) for IRS-1 and then assayed by immunoblot (B:) for IRS-1 or for phospho-Tyr (PY). Densitometric quantification of the immunoblot data is shown in the graph (*$p < 0.05$; mean ± SEM).

(B) As in (A), except that DIO *Camk2g*$^{fl/fl}$ mice treated with AAV-TBG-LacZ or AAV-TBG-Cre were used and p-IR was also assayed by IP/B (*$p < 0.05$; mean ± SEM).

(C) As in (B), except that DIO *Mapk14*$^{fl/fl}$ mice were used, and p-IRS-2 was also assayed by IP/B (*$p < 0.05$; mean ± SEM).

See also Figures S2 and S3.

Thus, CaMKII is both necessary and sufficient for the palmitate-induced insulin signaling defect in primary HCs.

We recently demonstrated that CaMKII mediates glucagon-induced HGP through p38-induced phosphorylation of FoxO1 on non-Akt sites (Ozcan et al., 2012). In particular, phosphorylation of FoxO1 by p38 promotes nuclear localization of FoxO1 and transcription of FoxO1 target genes involved in HGP, and inhibition of CaMKII or p38 leads to cytoplasmic localization of FoxO1 and inhibition of HGP. Because FoxO1 has been implicated in the regulation of Akt action (Lin and Accili, 2011), we investigated the contribution of FoxO1 nuclear exclusion in the enhancement of insulin signaling by CaMKII deficiency. We began with a series of experiments using nuclear FoxO1 restoration in palmitate-treated HCs. First, a nuclear FoxO1 bioassay—induction of the FoxO1 gene target *Igfbp1*—was used to verify our previous data (Ozcan et al., 2012) showing that deletion of CaMKIIγ caused a decrease in nuclear FoxO1 activity that could be restored by transduction with constitutively nuclear adeno-FoxO1-ADA (Figure S3A). We then used this model to ask whether nuclear FoxO1 restoration would abrogate the benefit of CaMKII deletion on insulin-induced p-Akt. As before, deletion of CaMKII improved insulin-induced p-Akt, and this improvement was not diminished by FoxO1 restoration (Figure S3B). These data indicate the distinct nature of the two CaMKII pathways.

We next investigated this important point in vivo. As in lean mice, adeno-K43A-CaMKII treatment markedly diminished nuclear FoxO1 in the livers of obese mice (Figure S3C). However, as was the case with HCs, restoration of nuclear FoxO1 did not reverse the benefit of CaMKII inhibition (K43A) on insulin-induced p-Akt (Figure S3D). Thus, the improvement in insulin-induced p-Akt by CaMKII deficiency is not due to nuclear exclusion of FoxO1. Rather, there appear to be two separate CaMKII pathways, one involved in CaMKII-p38-FoxO1-dependent HGP (Ozcan et al., 2012), and the other involved in defective insulin-induced p-Akt.

Inhibition of CaMKII or p38α Improves Insulin-Induced Akt Phosphorylation by Suppressing TRB3

In considering mechanisms of how insulin-induced p-Akt signaling distal to IRS proteins is regulated, we tested the role of the pseudokinase tribble 3 (TRB3), a molecule that is increased in the livers of obese mice and humans and was previously shown to bind to Akt and thereby prevent its

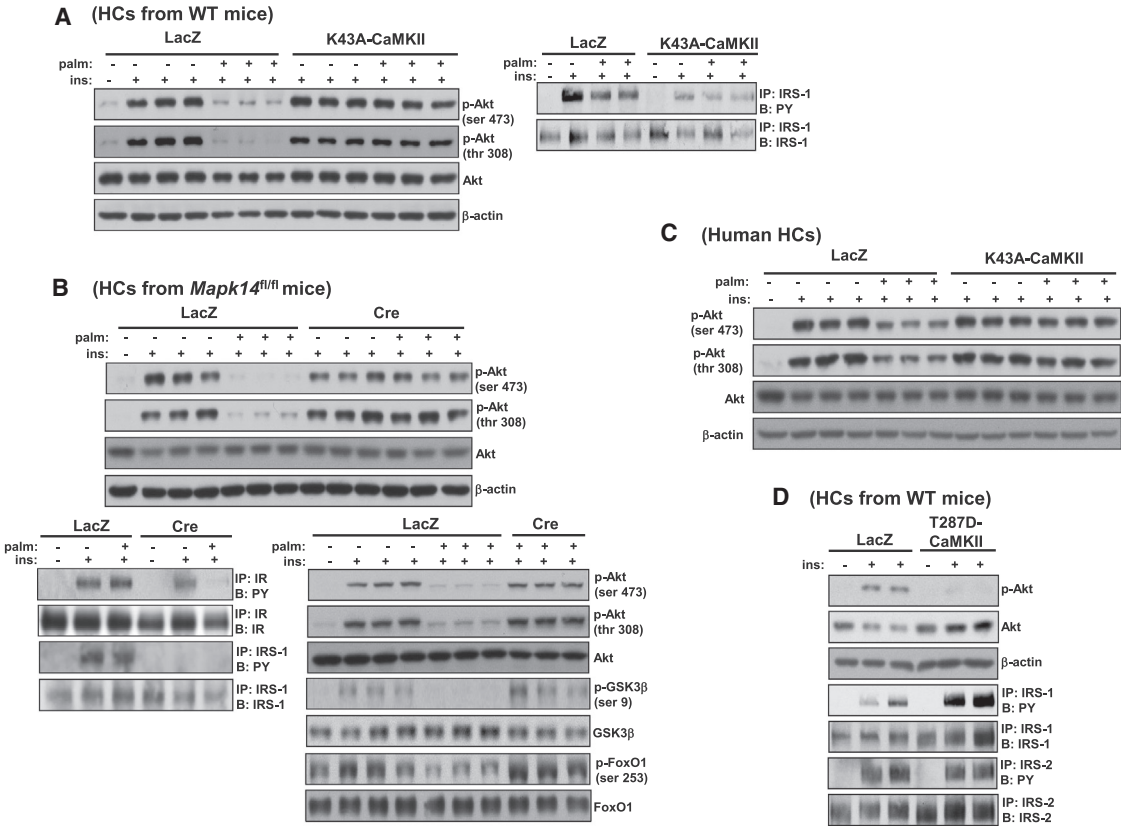

Figure 4. Inhibition of CaMKII or p38α Improves Insulin-Induced Akt Phosphorylation in Palmitate-Treated Primary Hepatocytes

(A) Primary HCs from WT mice were transduced with adeno-LacZ or adeno-K43A-CaMKII at an moi of 10 and then 24 hr later incubated with either BSA control or 0.2 mM palmitate for 19 hr, with the last 5 hr in serum-free media. The cells were then treated with 100 nM insulin or vehicle control for 5 min, and lysates were probed for p-Akt, total Akt, and β-actin by immunoblot (left panel) or immunoprecipitated for IRS-1 and then assayed by immunoblot for the total level of IRS-1 or for phospho-Tyr (PY) (right panel).

(B) HCs from *Mapk14*$^{fl/fl}$ mice were transduced with adeno-LacZ or adeno-Cre and 24 hr later incubated with palmitate and then insulin as in (A). Lysates were probed for p-Akt, total Akt, β-actin (upper panel), p-GSK3β, total GSK3β, p-FoxO1, and total FoxO1 by immunoblot or immunoprecipitated for IR and IRS-1 and then assayed by immunoblot for the total level of the respective proteins or for phospho-Tyr (lower panel).

(C) Primary human HCs (metabolism qualified) were transduced with adeno-LacZ or adeno-K43A-CaMKII at an moi of 30 and then 36 hr later incubated with either BSA control or 0.2 mM palmitate for 10 hr, with the last 5 hr in serum-free media. The cells were then treated with 100 nM insulin or vehicle control for 5 min, and lysates were probed for p-Akt, total Akt, and β-actin by immunoblot.

(D) As in (A), except adeno-T287D-CaMKII was used and IRS-2 was also assayed.

See also Figure S3.

phosphorylation by insulin (Du et al., 2003). We first investigated the effect of CaMKII and p38 deficiency on TRB3 levels in HCs. Palmitate treatment of control HCs led to an increase in TRB3 levels, consistent with a previous report (Cunha et al., 2012). Most importantly, CaMKII deficiency markedly decreased TRB3 protein and mRNA under both basal and palmitate-treated conditions (Figures 5A and S4A). To show relevance in vivo, we tested the effect of CaMKII deficiency or inhibition on TRB3 levels in obese mice. Consistent with the HC data, TRB3 levels were markedly suppressed in DIO *Camk2g*$^{-/-}$ mice or in *ob*/*ob* mice transduced with adeno-K43A-CaMKII (Figure 5B).

To test the importance of TRB3 in the enhancement of insulin-induced p-Akt conferred by CaMKII deficiency, we transduced DIO *Camk2g*$^{fl/fl}$ mice with TRB3 in order to bring TRB3 protein to a level similar to that in WT. TRB3 overexpression abrogated the improvement in insulin-induced p-Akt conferred by CaMKII deficiency (Figure S4B), indicating that the suppression of TRB3 by CaMKII deficiency is causally important in the improvement in insulin signaling. We then conducted a similar experiment except used physiologic refeeding (16 hr fasting followed by 4 hr of a high-fat diet feeding) instead of portal vein insulin injection to activate Akt. Similar to the case with portal vein insulin injections, TRB3 overexpression abolished the improvement in refeeding-induced p-Akt conferred by CaMKII inhibition (Figure 5C). In line with the effect of TRB3 restoration on insulin signaling, treatment of mice with adeno-TRB3 abrogated the lowering of blood glucose (Figure 5D) and plasma insulin (Figure 5E) by CaMKII inhibition in DIO mice under both fasting and refeeding conditions. Next, we sought to examine the effect of CaMKII deletion in TRB3-inhibited HCs. RNAi mediated knockdown of TRB3 in CaMKII-deficient HCs did not further improve insulin-induced p-Akt (Figure S4C), consistent with the idea that TRB3 is the downstream effector of CaMKII in the regulation of insulin-induced p-Akt.

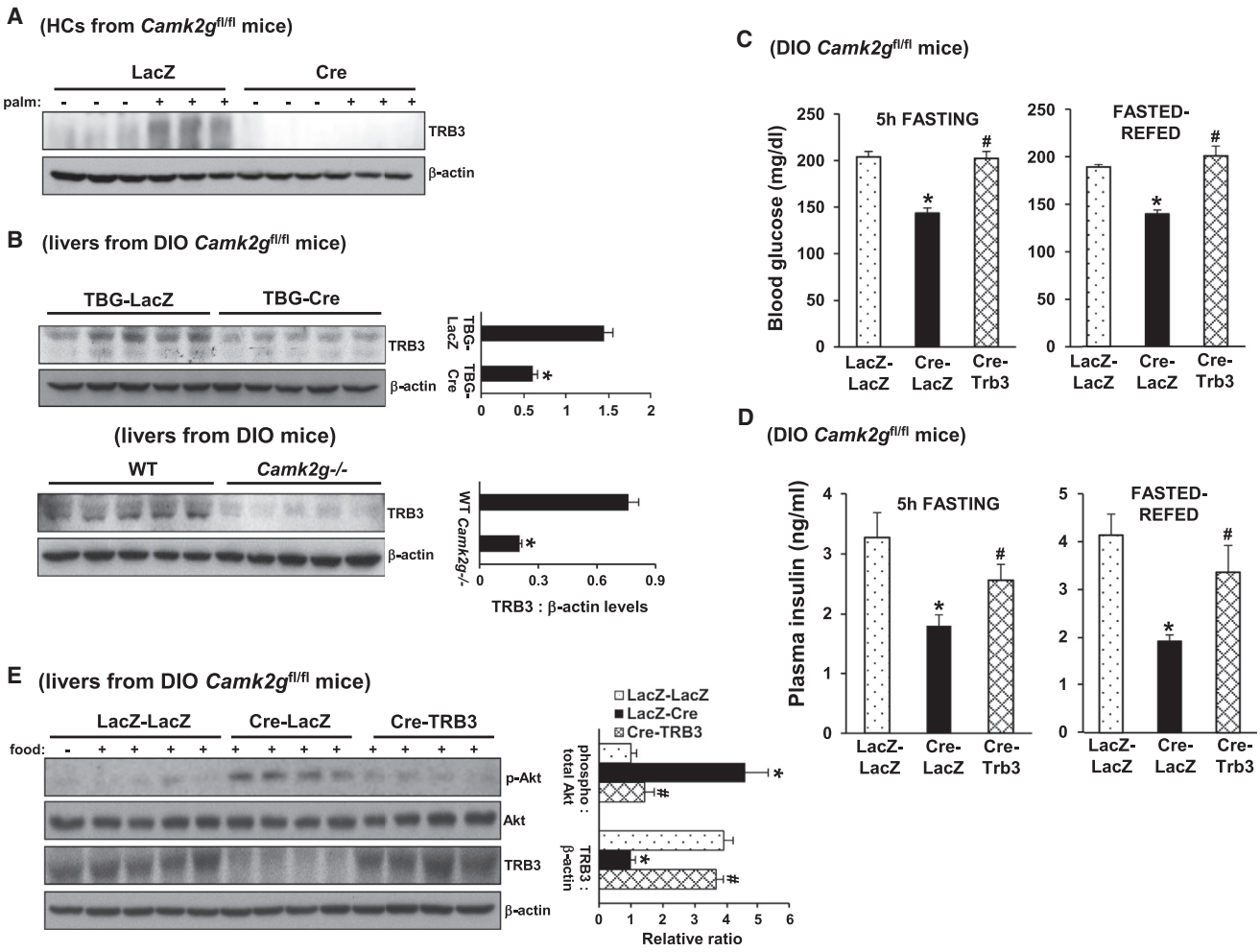

Figure 5. Improvement in Insulin-Induced Akt Phosphorylation and Glucose Homeostasis by CaMKII Deficiency Are Abrogated by Restoring TRB3

(A) HCs from *Camk2g*$^{fl/fl}$ mice were transduced with adeno-LacZ or adeno-Cre and then 24 hr later incubated with BSA or palmitate (0.2 mM) for 19 hr. Lysates were immunoblotted for TRB3 and β-actin.

(B) TRB3 and β-actin were probed in livers from DIO WT mice, *Camk2g*$^{-/-}$ mice, or *Camk2g*$^{fl/fl}$ mice treated with TBG-LacZ or TBG-Cre. Densitometric quantification of the immunoblot data is shown in the graph (*$p < 0.05$; mean ± SEM).

(C–E) DIO *Camk2g*$^{fl/fl}$ mice were treated with TBG-Cre or TBG-LacZ, and 5 days later half of the TBG-LacZ mice received adeno-TRB3, while the other half received adeno-LacZ control. After 4 weeks, 5 hr fasting and fasted-refed blood glucose and plasma insulin were assayed. One week later, livers were assayed for p-Akt, total Akt, TRB3, β-actin by immunoblotting after fasting the mice for 16 hr and then refeeding for 4 hr. Differing symbols indicate $p < 0.05$; mean ± SEM. See also Figure S4.

The data in our previous report (Ozcan et al., 2012) and here indicate that, in the setting of obesity, CaMKIIγ deficiency lowers HGP by suppressing p38-mediated FoxO1 nuclear localization and improves insulin signaling by suppressing hepatic TRB3 expression, which then leads to improvement in insulin/Akt signaling. We showed above that nuclear FoxO1 does not affect insulin-induced p-Akt. However, an interesting question is whether the improvement in p-Akt (new pathway here) contributes, via Akt phosphorylation sites on FoxO1 (Lin and Accili, 2011), to nuclear exclusion of FoxO1 in obese mice lacking CaMKII or p38. To address this issue, we disabled the improvement in p-Akt in CaMKII-deficient obese mice through TRB3 restoration (above). As predicted by the idea that both pathways contribute to the exclusion of nuclear FoxO1 by CaMKII deficiency in the setting of obesity, TRB3 restoration in CaMKII-deficient mice led to a partial increase in nuclear FoxO1 (Figure S4D). We then reasoned that we should be able to show no effect of TRB3 on nuclear FoxO1 if we chose a non-insulin-resistant model; i.e., a model where TRB3 would be irrelevant in terms of the Akt-FoxO1 pathway. For this purpose, we used non-insulin-resistant forskolin-treated HCs (Ozcan et al., 2012). Nuclear FoxO1 biological activity was assayed by quantifying the mRNA levels of the FoxO1 target genes, *G6pc* and *Pck1*. In this case, as predicted, the suppressive effect of CaMKIIγ deficiency on forskolin-induced *G6Pc* and *Pck1* mRNA was not abrogated by transduction with adeno-TRB3 (Figure S4E). Thus, in the absence of a defect in insulin signaling, TRB3 restoration does not affect the ability of CaMKII deficiency to suppress HGP gene induction.

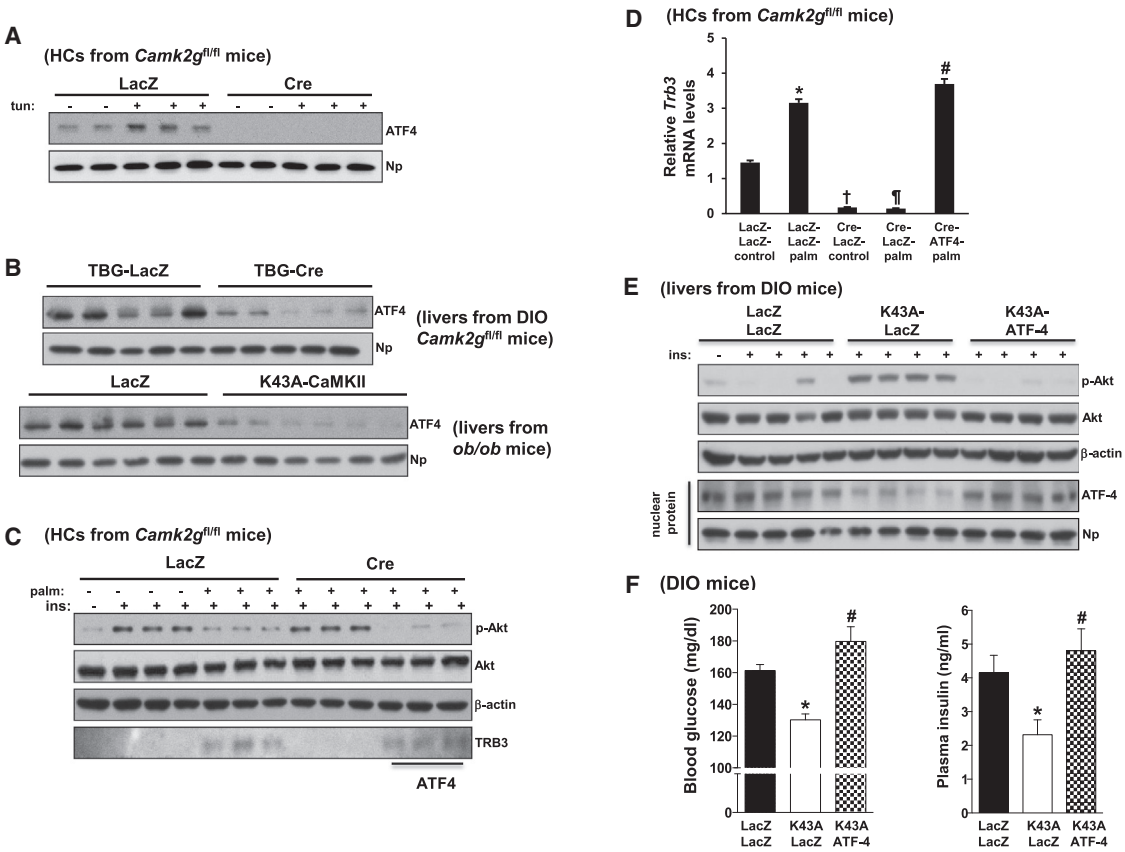

Figure 6. Improvement in Insulin-Induced Akt Phosphorylation and Glucose Homeostasis by CaMKII Deficiency Are Abrogated by Restoring ATF4

(A) HCs from *Camk2g*$^{fl/fl}$ mice were transduced with adeno-LacZ or adeno-Cre. Twenty-four hours later, cells were incubated with tunicamycin (0.5 μg/ml) or vehicle control for 4 hr. Nuclear lysates were immunoblotted for ATF4 and nucleophosmin (Np) as a loading control.

(B) Nuclear ATF4 and nucleophosmin (Np) were probed in livers from DIO *Camk2g*$^{fl/fl}$ mice treated with TBG-Cre or TBG-LacZ or *ob/ob* mice treated with adeno-LacZ or adeno-K43A-CaMKII.

(C) HCs from *Camk2g*$^{fl/fl}$ mice were transduced with adeno-LacZ or adeno-Cre, and then 4 hr later half of the adeno-Cre transduced cells received adeno-ATF4, while the other half received adeno-LacZ control. After 24 hr, the cells were incubated with palmitate, and then insulin-induced p-Akt was assayed as in Figure 4.

(D) As in (C), except that *Trb3* mRNA was assayed by RT-qPCR (bars with different symbols are different from each other and control, $p < 0.01$; mean ± SEM).

(E and F) Sixteen-week-old DIO mice were administered adeno-LacZ or adeno-K43A-CaMKII, and then 2 days later half of the adeno-K43A-CaMKII mice received adeno-ATF4, while the other half received adeno-LacZ control. Livers were assayed for p-Akt, total Akt, β-actin, and nuclear ATF4 and nucleophosmin (Np) by immunoblotting after insulin injection through portal vein. Five hour fasting blood glucose and plasma insulin were assayed after 3 weeks of treatment (bars with different symbols are different from each other and from control, $p < 0.05$; mean ± SEM).

See also Figure S5.

These data further establish the separateness of the two CaMKII/p38 pathways, although in the setting of insulin resistance, FoxO1 nuclear localization is promoted by both pathways.

CaMKII Deficiency Suppresses TRB3 by Decreasing ER Stress-Induced ATF4

TRB3 expression has been reported to be increased in cancer cells and pancreatic islets undergoing ER stress (Bromati et al., 2011; Corcoran et al., 2005). Moreover, in HEK293 embryonic kidney cells treated with tunicamycin, a glycosylation inhibitor that activates the unfolded protein response (UPR), TRB3 was shown to be a direct transcriptional target of the ER stress-inducible transcription factor ATF4 (Ohoka et al., 2005). Because hepatic ER stress is increased obesity and may act as a link between obesity and insulin resistance (Gregor et al., 2009; Ozcan et al., 2004), we reasoned that a CaMKII-ATF4-TRB3 pathway might be upstream of defective insulin-induced p-Akt in obese liver. We first measured ATF4 levels in WT versus CaMKIIγ-deficient HCs under various conditions. Exposure to tunicamycin increased ATF4 in control HCs, but not in CaMKII-deficient HCs (Figure 6A). Similarly, the livers of obese mice deficient in hepatic CaMKIIγ had lower ATF4 levels compared with obese WT mice (Figure 6B), suggesting that CaMKII might be suppressing TRB3 by first suppressing ATF4. To test this possibility and link it to insulin-induced p-Akt, palmitate-treated CaMKIIγ-deficient HCs were transduced with adeno-ATF4 to restore the level of this protein to the WT level. Consistent with our hypothesis, ATF4 restoration resulted in an increase in TRB3 mRNA and protein levels and abrogation of the improvement in p-Akt seen with CaMKII deficiency (Figures 6C and 6D). To further validate the

importance of ATF4 suppression in the improvement of insulin signaling by CaMKII deficiency, we restored ATF4 in adeno-K43A-CaMKII-treated DIO mice. We observed that the beneficial effect of CaMKIIγ inhibition on insulin-induced p-Akt was abrogated by transduction with adeno-ATF4 (Figure 6E). Consistent with the effect of ATF4 restoration on insulin signaling, the blood-glucose- and plasma-insulin-lowering effect of CaMKII inhibition in DIO mice was also abrogated by adeno-ATF4 (Figure 6F). These data support a signaling pathway in which CaMKII promotes ATF4 expression, which in turn induces TRB3, leading to suppression of insulin-induced p-Akt.

ATF4 is translationally upregulated when the PERK branch of the UPR is activated (Tabas and Ron, 2011; Walter and Ron, 2011). We therefore investigated whether CaMKII deficiency suppresses PERK activation as a mechanism for reduced ATF-4 and TRB3 expression. When exposed to tunicamycin, HCs lacking CaMKIIγ showed a marked decrease in PERK phosphorylation, which is a measure of its activation, as well as decreased expression of the ATF4 gene target CEBP/β-homologous protein (CHOP) (Figure S5A). Similar results were seen with tunicamycin- or palmitate-treated HCs deficient in CaMKIIγ or p38α (Figures S5B and S5C). To explore a possible role of CaMKII in the regulation of PERK branch of UPR in vivo, we analyzed *Chop* mRNA levels in obese mice. Consistent with our in vitro data, obese mice deficient in hepatic CaMKII had lower *Chop* mRNA levels in liver compared with WT mice (Figure S5D). Interestingly, the IRE1α branch of the UPR, as measured by *Xbp1* mRNA splicing, was not activated either in palmitate-treated HCs or in obese mouse liver (Figures S5E and S5F). Thus, CaMKII deficiency selectively suppresses the PERK branch of the UPR in the setting of obesity, leading to decreased ATF4 and TRB3 and increased insulin-induced p-Akt.

Evidence that an ATF6-p58^{IPK} Pathway Is Upstream of the ATF4-TRB3-Akt Pathway

We next addressed how silencing of CaMKII might suppress the PERK branch of the UPR. We focused on the idea that CaMKII deficiency might increase the expression of a widely studied inhibitor of PERK kinase called p58^{IPK} (Yan et al., 2002). Initial support for this idea came from the finding that p58^{IPK} mRNA and protein levels were increased by CaMKIIγ or p38α deficiency in ER-stressed HCs and obese mice liver (Figures 7A and S6A–S6C). Most importantly, siRNA-mediated silencing of p58^{IPK} increased *Trb3* and abrogated the improvement in insulin-Akt signaling in CaMKII-deficient, palmitate-treated HCs (Figures 7B and 7C), demonstrating a casual link between the proposed upstream role of p58^{IPK} and the key functional endpoint of the CaMKII pathway, insulin-induced p-Akt.

Finally, to explore how CaMKII deficiency might increase p58^{IPK} in obese mice liver, we explored the role of a known inducer of the molecule, ATF6, which has been shown to be decreased in the livers of obese mice (Wang et al., 2009; Wu et al., 2007). This hypothesis predicts that CaMKII deficiency would increase ATF6 levels, which was the case in obese liver and in tunicamycin- and palmitate-treated HCs (Figures 7D, S6D, and 7F). To determine causation, we silenced *Atf6* in palmitate-treated CaMKII-deficient HCs using siRNA and found that this treatment lowered *p58^{ipk}*, increased *Trb3*, and reduced insulin-induced p-Akt to the level of palmitate-treated control HCs (Figures 7E and 7F). Thus, inhibition of hepatic CaMKII improves insulin signaling in the setting of obesity through induction of ATF6 and p58^{IPK}, which suppresses the PERK-ATF4-TRB3 pathway.

DISCUSSION

The epidemic of obesity and T2D demands a precise understanding of the molecular events that link obesity to the two cardinal features of T2D: hyperglycemia and insulin resistance. The current findings, viewed together with our two recent studies (Ozcan et al., 2012; Wang et al., 2012), present a unified scheme in which cytosolic calcium working through CaMKII in the liver plays a central role (Figure 7G). Cytosolic calcium in the liver is elevated in obesity through at least two mechanisms: (1) lipid-induced deactivation of the calcium pump SERCA (Fu et al., 2011; Park et al., 2010) and (2) opening of the IP3R ER calcium channel by two processes triggered by glucagon receptor activation, formation of IP3 by phospholipase C (Hansen et al., 1998) and direct activation of the channel by PKA-mediated phosphorylation of IP3R (Wang et al., 2012). With regard to excessive HGP as a cause of hyperglycemia, the released calcium activates both calcineurin, which promotes nuclear localization of CRTC2 (Wang et al., 2012), and CaMKII, which, through p38, promotes nuclear localization of FoxO1 (Ozcan et al., 2012). The current report reveals that a separate pathway in the liver, also mediated by CaMKII-p38, disrupts insulin-induced Akt phosphorylation, which is a key process in the pathogenesis of insulin resistance (Brozinick et al., 2003; Cho et al., 2001; Krook et al., 1998). From a translational viewpoint, this scheme suggests that a single pathway could be therapeutically inhibited to achieve improvement in both hyperglycemia and insulin resistance in obesity and T2D.

The key downstream step through which CaMKII deficiency improves insulin-induced p-Akt is suppression of TRB3, which binds Akt, prevents its membrane association, and thus blocks its phosphorylation (Du et al., 2003). TRB3 levels are increased in the livers of obese mice and humans, and it has been proposed to play a major role in hepatic insulin resistance in this setting (Du et al., 2003; Lima et al., 2009). Notably, when TRB3 is expressed in WT mouse liver to a level similar to that observed in obese mouse liver, insulin resistance occurs, whereas silencing its expression in obesity improves glucose tolerance (Du et al., 2003). Moreover, a common gain-of-function polymorphism in TRB3 (Q48R) that increases the ability of TRB3 to suppress insulin-induced p-Akt is associated with an increase in insulin-resistant syndromes in several independent cohorts (Prudente et al., 2005). TRB3 may also play a role in adipose tissue, because TRB3 antisense oligonucleotide (ASO) treatment of obese rats was reported to improve insulin sensitivity through a mechanism that involved activation of PPAR-γ and changes in adipogenesis rather than an increase in p-Akt (Weismann et al., 2011). In the case of the CaMKII pathway, the hepatic p-Akt mechanism is clearly important, but whether changes in PPARγ and adipogenesis also occur remains to be investigated.

An important finding in our study is that CaMKII induces TRB3 through activation of the PERK-ATF4 branch of UPR, providing a link between CaMKII and ER stress. In the context of previous findings linking P58^{IPK} to suppression of PERK activation (Yan et al., 2002), our data suggest that the obesity-induced

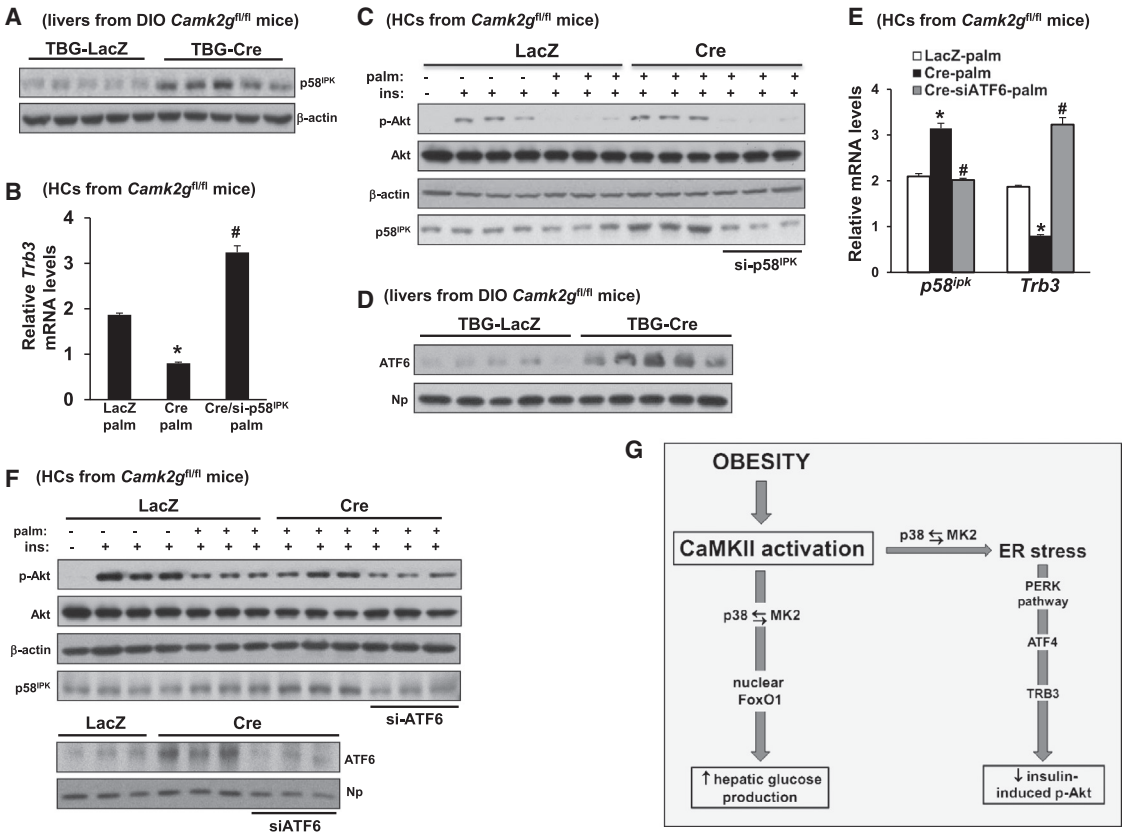

Figure 7. Acute Insulin-Induced p-Akt Enhancement in *Camk2g*$^{-/-}$ Hepatocytes Is Partially Abrogated by ATF6 Inhibition

(A) p58^{IPK} and β-actin were probed by immunoblot in livers from DIO *Camk2g*$^{fl/fl}$ mice treated with AAV-TBG-Cre or AAV-TBG-LacZ.

(B) HCs from *Camk2g*$^{fl/fl}$ mice were pretreated with either scrambled RNA (first two bars) or siRNA targeting *p58*^{ipk} (si-p58). After 12 hr, the cells were transduced with adeno-LacZ or adeno-Cre. After an additional 24 hr, the cells were incubated with BSA control or palmitate (0.2 mM) for 19 hr, with the last 5 hr in serum-free media. The cells were then assayed for *Trb3* mRNA by RT-qPCR (bars with different symbols are different from each other and control, $p < 0.05$; mean ± SEM).

(C) As in (B), except the cells were then treated with ± 100 nM insulin for 5 min, and lysates were immunoblotted for p-Akt, total Akt, β-actin, and p58^{IPK} by immunoblot.

(D) Nuclear ATF6 and nucleophosmin (Np) were probed by immunoblot in livers from DIO *Camk2g*$^{fl/fl}$ mice treated with AAV-TBG-Cre or AAV-TBG-LacZ.

(E) As in (B), except siRNA targeting *Atf6* (siATF6) was used, and *p58*^{ipk} mRNA was also assayed; the first two bars in each group received scrambled RNA (bars with different symbols are different from each other and control, $p < 0.05$; mean ± SEM).

(F) HCs were prepared as in (C), except siRNA targeting *Atf6* (siATF6) was used. Lysates were immunoblotted for p-Akt, total Akt, β-actin, and p58^{IPK} by immunoblot. In the lower blot, nuclei from a parallel set of cells treated with palmitate were probed for ATF6 and nucleophosmin (Np) by immunoblot.

(G) The data here and previously (Ozcan et al., 2012) support an integrated scheme in which CaMKII mediates two key pathways in the setting of obesity, one contributing to defective insulin signaling and the other to excessive HGP. Thus, inhibition of liver CaMKII or its downstream agent p38 improves the two cardinal features of T2D.

See also Figure S6.

CaMKII/p38 pathway activates PERK through suppression of p58^{IPK}. Interestingly, p58^{IPK}-deficient mice exhibit glucosuria and hyperglycemia through a mechanism attributed to β cell dysfunction, suggesting the p58^{IPK} protects β cells (Ladiges et al., 2005). Our results now reveal another potential beneficial effect of p58^{IPK} in metabolism, namely improvement in hepatic insulin signaling through suppression of CaMKII-induced ATF4 and TRB3.

We show that a key link between CaMKII/p38 deficiency and P58^{IPK} induction is ATF6. CaMKII-deficient obese mice have higher nuclear ATF6 levels, and silencing ATF6 in these mice lowers p58^{IPK} and suppresses insulin-induced p-Akt. How inhibition of the CaMKII/p38 pathway leads to increased ATF6 expression remains to be elucidated, but it is interesting to consider previous studies linking CaMKII/p38 activation with changes in gene expression (Backs et al., 2006; Raingeaud et al., 1996). As with p58^{IPK} induction and TRB3 suppression, ATF6 activation may have additional and independent beneficial effects in obesity and T2D. In particular, Montminy and colleagues have provided evidence that ATF6 could suppress HGP through disruption of CREB-CRTC2 interaction (Wang et al., 2009).

The discovery of a common pathway that independently affects the two cardinal features of T2D raises the possibility of new therapeutic targets. To the extent that excessive glucagon signaling is at least one mechanism that likely activates the

CaMKII-p38-MK2 pathway in T2D, relevance to humans is suggested by the ability of glucagon receptor antagonists (GRAs) to markedly lower blood sugar in human subjects (Petersen and Sullivan, 2001). However, there may be an advantage to targeting a more downstream branch of the glucagon pathway in order to avoid the possible adverse effects of GRAs (Yang et al., 2011). In terms of the "druggability" of the molecules in the pathway, CaMKII inhibitors are in development for heart failure (Rokita and Anderson, 2012), and MK2 inhibitors are being explored as a more effective alternative than p38 inhibitors for inflammatory diseases (Huang et al., 2012). Because all new diabetes drugs must pass safety tests for coronary artery disease, the applications of these inhibitors to T2D may be particularly advantageous: CaMKII inhibition in liver lowers plasma cholesterol and triglycerides in obese mice; CaMKII inhibition in macrophages protects the cells from ER stress-induced apoptosis, a key step in advanced plaque progression (Timmins et al., 2009); and MK2-deficient *Ldlr*$^{-/-}$ mice are protected against atherosclerosis (Jagavelu et al., 2007).

EXPERIMENTAL PROCEDURES

Mouse Experiments

Camk2g$^{-/-}$ mice were generated as described previously (Backs et al., 2010) and crossed onto the C57BL6/J background. *Camk2g*$^{fl/fl}$ mice were generated by flanking exon 1–2 with *loxP* sites, which will be described in detail elsewhere (M. Kreuβer, J.B., and E.N.O., unpublished data). *Ob/ob* mice were obtained from The Jackson Laboratory. *Mapk14*$^{fl/fl}$ mice were generated as described previously (Engel et al., 2005) and generously provided by Dr. Yibin Wang, UCLA School of Medicine. Male mice were fed a standard chow diet or a high-fat diet with 60% kcal from fat (Research Diets) and maintained on a 12 hr light-dark cycle. Recombinant adenovirus (0.5–3 × 10^9 plaque-forming units/mice) was delivered by tail vein injection, and experiments were commenced after 5–7 days. Fasting blood glucose was measured in mice that were fasted for 4–6 hr, with free access to water, using a glucose meter. Glucose tolerance tests were performed in overnight-fasted mice by assaying blood glucose at various times after i.p. injection of glucose (0.5 g/kg for *ob/ob* and 1.5 g/kg for DIO). Plasma insulin levels were measured using ultrasensitive mouse insulin ELISA Kit (Crystal Chem). Insulin tolerance tests were performed in 5 hr-fasted mice by assaying blood glucose at various times after i.p. injection of insulin (2 IU/kg for *ob/ob* and 0.75–1 IU/kg for DIO). Animal studies were performed in accordance with the Columbia University Institutional Animal Care and Use Committee.

Portal Vein Insulin Infusion and Protein Extraction from Tissues

Following 6 hr food withdrawal, mice were anesthetized, and insulin (1–2 IU/kg) or PBS was injected into mice through the portal vein. Three minutes after injection, tissues were removed, frozen in liquid nitrogen, and kept at −80°C until processing. For protein extraction, tissues were placed in a cold lysis buffer (25 mM Tris-HCl [pH 7.4], 1 mM EGTA, 1 mM EDTA, 10 mM $Na_4P_2O_7$, 10 mM NaF, 2 mM Na_3VO_4, 1% NP-40, 2 mM PMSF, 5 μg/ml leupeptin, 10 nM okadaic acid, and 5 μg/ml aprotinin). After homogenization on ice, the tissue lysates were centrifuged, and the supernatant fractions were used for immunoblot analysis.

Primary Hepatocytes

Primary mouse hepatocytes (HCs) were isolated from 8- to 12-week-old mice as described previously (Ozcan et al., 2012). For most experiments, the HCs were cultured in DMEM containing 10% fetal bovine serum, treated as described in the figure legends, and then incubated for 5 hr in serum-free DMEM. HCs were transduced with adenoviral constructs 4 hr after plating, and experiments were conducted 12 hr after transduction. Transfections with scrambled RNA and siRNAs targeting *p58*^{ipk} and *Atf6* were carried out using Lipofectamine RNAiMAX transfection reagent (Life Technologies, Inc.) according to the manufacturer's instructions. Metabolism-qualified human HCs were purchased from Life Technologies and cultured according to the manufacturer's instructions.

Statistical Analysis

All results are presented as mean ± SEM. p values were calculated using the Student's t test for normally distributed data and the Mann-Whitney rank sum test for nonnormally distributed data.

SUPPLEMENTAL INFORMATION

Supplemental Information includes six figures and Supplemental Experimental Procedures and can be found with this article at http://dx.doi.org/10.1016/j.cmet.2013.10.011.

ACKNOWLEDGMENTS

We thank Dr. Harold A. Singer (Albany Medical College) for adeno-LacZ, T287D-CaMKII, and K43A-CaMKII; Dr. Marc Montminy (Salk Institute for Biological Studies) for adeno-TRB3 and adeno-TRB3 RNAi; Randal J. Kaufman (Sanford-Burnham Medical Research Institute) for adeno-ATF4; and Dr. Domenico Accili (Columbia University) for adeno-FoxO1-ADA. This work was supported by an American Heart Association Scientist Development Grant (11SDG5300022) and a NYONRC Pilot and Feasibility Grant (DK26687) to L.O.; by FAPESP/BEPE 2012/21290-4 to J.C.S.; by the DZHK (German Centre for Cardiovascular Research), BMBF (German Ministry of Education and Research), DFG (Deutsche Forschungsgemeinschaft; BA 2258/2-1), and the European Commission (FP7-Health-2010; MEDIA-261409) to J.B.; and by NIH grants HL087123 and HL075662 to I.T. Authors L.O. and I.T. are in the group of cofounders of Tabomedex Biosciences LLC, which is developing inhibitors of the pathway described in this report for treatment of type 2 diabetes.

Received: April 11, 2013
Revised: September 7, 2013
Accepted: October 11, 2013
Published: November 21, 2013

REFERENCES

Achard, C.S., and Laybutt, D.R. (2012). Lipid-induced endoplasmic reticulum stress in liver cells results in two distinct outcomes: adaptation with enhanced insulin signaling or insulin resistance. Endocrinology *153*, 2164–2177.

Backs, J., Song, K., Bezprozvannaya, S., Chang, S., and Olson, E.N. (2006). CaM kinase II selectively signals to histone deacetylase 4 during cardiomyocyte hypertrophy. J. Clin. Invest. *116*, 1853–1864.

Backs, J., Stein, P., Backs, T., Duncan, F.E., Grueter, C.E., McAnally, J., Qi, X., Schultz, R.M., and Olson, E.N. (2010). The gamma isoform of CaM kinase II controls mouse egg activation by regulating cell cycle resumption. Proc. Natl. Acad. Sci. USA *107*, 81–86.

Bornfeldt, K.E., and Tabas, I. (2011). Insulin resistance, hyperglycemia, and atherosclerosis. Cell Metab. *14*, 575–585.

Bromati, C.R., Lellis-Santos, C., Yamanaka, T.S., Nogueira, T.C., Leonelli, M., Caperuto, L.C., Gorjão, R., Leite, A.R., Anhê, G.F., and Bordin, S. (2011). UPR induces transient burst of apoptosis in islets of early lactating rats through reduced AKT phosphorylation via ATF4/CHOP stimulation of TRB3 expression. Am. J. Physiol. Regul. Integr. Comp. Physiol. *300*, R92–R100.

Brown, M.S., and Goldstein, J.L. (2008). Selective versus total insulin resistance: a pathogenic paradox. Cell Metab. *7*, 95–96.

Brozinick, J.T., Jr., Roberts, B.R., and Dohm, G.L. (2003). Defective signaling through Akt-2 and -3 but not Akt-1 in insulin-resistant human skeletal muscle: potential role in insulin resistance. Diabetes *52*, 935–941.

Cho, H., Mu, J., Kim, J.K., Thorvaldsen, J.L., Chu, Q., Crenshaw, E.B., 3rd, Kaestner, K.H., Bartolomei, M.S., Shulman, G.I., and Birnbaum, M.J. (2001). Insulin resistance and a diabetes mellitus-like syndrome in mice lacking the protein kinase Akt2 (PKB beta). Science *292*, 1728–1731.

Corcoran, C.A., Luo, X., He, Q., Jiang, C., Huang, Y., and Sheikh, M.S. (2005). Genotoxic and endoplasmic reticulum stresses differentially regulate TRB3 expression. Cancer Biol. Ther. *4*, 1063–1067.

Cunha, D.A., Igoillo-Esteve, M., Gurzov, E.N., Germano, C.M., Naamane, N., Marhfour, I., Fukaya, M., Vanderwinden, J.M., Gysemans, C., Mathieu, C., et al. (2012). Death protein 5 and p53-upregulated modulator of apoptosis mediate the endoplasmic reticulum stress-mitochondrial dialog triggering lipotoxic rodent and human β-cell apoptosis. Diabetes *61*, 2763–2775.

Du, K., Herzig, S., Kulkarni, R.N., and Montminy, M. (2003). TRB3: a tribbles homolog that inhibits Akt/PKB activation by insulin in liver. Science *300*, 1574–1577.

Engel, F.B., Schebesta, M., Duong, M.T., Lu, G., Ren, S., Madwed, J.B., Jiang, H., Wang, Y., and Keating, M.T. (2005). p38 MAP kinase inhibition enables proliferation of adult mammalian cardiomyocytes. Genes Dev. *19*, 1175–1187.

Freshney, N.W., Rawlinson, L., Guesdon, F., Jones, E., Cowley, S., Hsuan, J., and Saklatvala, J. (1994). Interleukin-1 activates a novel protein kinase cascade that results in the phosphorylation of Hsp27. Cell *78*, 1039–1049.

Fu, S., Yang, L., Li, P., Hofmann, O., Dicker, L., Hide, W., Lin, X., Watkins, S.M., Ivanov, A.R., and Hotamisligil, G.S. (2011). Aberrant lipid metabolism disrupts calcium homeostasis causing liver endoplasmic reticulum stress in obesity. Nature *473*, 528–531.

Gaestel, M. (2006). MAPKAP kinases—MKs—two's company, three's a crowd. Nat. Rev. Mol. Cell Biol. *7*, 120–130.

Gregor, M.F., Yang, L., Fabbrini, E., Mohammed, B.S., Eagon, J.C., Hotamisligil, G.S., and Klein, S. (2009). Endoplasmic reticulum stress is reduced in tissues of obese subjects after weight loss. Diabetes *58*, 693–700.

Hansen, L.H., Gromada, J., Bouchelouche, P., Whitmore, T., Jelinek, L., Kindsvogel, W., and Nishimura, E. (1998). Glucagon-mediated Ca2+ signaling in BHK cells expressing cloned human glucagon receptors. Am. J. Physiol. *274*, C1552–C1562.

Hemi, R., Yochananov, Y., Barhod, E., Kasher-Meron, M., Karasik, A., Tirosh, A., and Kanety, H. (2011). p38 mitogen-activated protein kinase-dependent transactivation of ErbB receptor family: a novel common mechanism for stress-induced IRS-1 serine phosphorylation and insulin resistance. Diabetes *60*, 1134–1145.

Huang, X., Zhu, X., Chen, X., Zhou, W., Xiao, D., Degrado, S., Aslanian, R., Fossetta, J., Lundell, D., Tian, F., et al. (2012). A three-step protocol for lead optimization: quick identification of key conformational features and functional groups in the SAR studies of non-ATP competitive MK2 (MAPKAPK2) inhibitors. Bioorg. Med. Chem. Lett. *22*, 65–70.

Jagavelu, K., Tietge, U.J., Gaestel, M., Drexler, H., Schieffer, B., and Bavendiek, U. (2007). Systemic deficiency of the MAP kinase-activated protein kinase 2 reduces atherosclerosis in hypercholesterolemic mice. Circ. Res. *101*, 1104–1112.

Könner, A.C., and Brüning, J.C. (2012). Selective insulin and leptin resistance in metabolic disorders. Cell Metab. *16*, 144–152.

Krook, A., Roth, R.A., Jiang, X.J., Zierath, J.R., and Wallberg-Henriksson, H. (1998). Insulin-stimulated Akt kinase activity is reduced in skeletal muscle from NIDDM subjects. Diabetes *47*, 1281–1286.

Ladiges, W.C., Knoblaugh, S.E., Morton, J.F., Korth, M.J., Sopher, B.L., Baskin, C.R., MacAuley, A., Goodman, A.G., LeBoeuf, R.C., and Katze, M.G. (2005). Pancreatic beta-cell failure and diabetes in mice with a deletion mutation of the endoplasmic reticulum molecular chaperone gene P58IPK. Diabetes *54*, 1074–1081.

Leavens, K.F., and Birnbaum, M.J. (2011). Insulin signaling to hepatic lipid metabolism in health and disease. Crit. Rev. Biochem. Mol. Biol. *46*, 200–215.

Lima, A.F., Ropelle, E.R., Pauli, J.R., Cintra, D.E., Frederico, M.J., Pinho, R.A., Velloso, L.A., and De Souza, C.T. (2009). Acute exercise reduces insulin resistance-induced TRB3 expression and amelioration of the hepatic production of glucose in the liver of diabetic mice. J. Cell. Physiol. *221*, 92–97.

Lin, H.V., and Accili, D. (2011). Hormonal regulation of hepatic glucose production in health and disease. Cell Metab. *14*, 9–19.

Ohoka, N., Yoshii, S., Hattori, T., Onozaki, K., and Hayashi, H. (2005). TRB3, a novel ER stress-inducible gene, is induced via ATF4-CHOP pathway and is involved in cell death. EMBO J. *24*, 1243–1255.

Ozcan, U., Cao, Q., Yilmaz, E., Lee, A.H., Iwakoshi, N.N., Ozdelen, E., Tuncman, G., Görgün, C., Glimcher, L.H., and Hotamisligil, G.S. (2004). Endoplasmic reticulum stress links obesity, insulin action, and type 2 diabetes. Science *306*, 457–461.

Ozcan, L., Wong, C.C., Li, G., Xu, T., Pajvani, U., Park, S.K., Wronska, A., Chen, B.X., Marks, A.R., Fukamizu, A., et al. (2012). Calcium signaling through CaMKII regulates hepatic glucose production in fasting and obesity. Cell Metab. *15*, 739–751.

Park, S.W., Zhou, Y., Lee, J., Lee, J., and Ozcan, U. (2010). Sarco(endo)plasmic reticulum Ca2+-ATPase 2b is a major regulator of endoplasmic reticulum stress and glucose homeostasis in obesity. Proc. Natl. Acad. Sci. USA *107*, 19320–19325.

Petersen, K.F., and Sullivan, J.T. (2001). Effects of a novel glucagon receptor antagonist (Bay 27-9955) on glucagon-stimulated glucose production in humans. Diabetologia *44*, 2018–2024.

Pfleiderer, P.J., Lu, K.K., Crow, M.T., Keller, R.S., and Singer, H.A. (2004). Modulation of vascular smooth muscle cell migration by calcium/ calmodulin-dependent protein kinase II-delta 2. Am. J. Physiol. Cell Physiol. *286*, C1238–C1245.

Prudente, S., Hribal, M.L., Flex, E., Turchi, F., Morini, E., De Cosmo, S., Bacci, S., Tassi, V., Cardellini, M., Lauro, R., et al. (2005). The functional Q84R polymorphism of mammalian Tribbles homolog TRB3 is associated with insulin resistance and related cardiovascular risk in Caucasians from Italy. Diabetes *54*, 2807–2811.

Raingeaud, J., Whitmarsh, A.J., Barrett, T., Dérijard, B., and Davis, R.J. (1996). MKK3- and MKK6-regulated gene expression is mediated by the p38 mitogen-activated protein kinase signal transduction pathway. Mol. Cell. Biol. *16*, 1247–1255.

Rokita, A.G., and Anderson, M.E. (2012). New therapeutic targets in cardiology: arrhythmias and Ca2+/calmodulin-dependent kinase II (CaMKII). Circulation *126*, 2125–2139.

Rouse, J., Cohen, P., Trigon, S., Morange, M., Alonso-Llamazares, A., Zamanillo, D., Hunt, T., and Nebreda, A.R. (1994). A novel kinase cascade triggered by stress and heat shock that stimulates MAPKAP kinase-2 and phosphorylation of the small heat shock proteins. Cell *78*, 1027–1037.

Saad, M.J., Araki, E., Miralpeix, M., Rothenberg, P.L., White, M.F., and Kahn, C.R. (1992). Regulation of insulin receptor substrate-1 in liver and muscle of animal models of insulin resistance. J. Clin. Invest. *90*, 1839–1849.

Saltiel, A.R., and Kahn, C.R. (2001). Insulin signalling and the regulation of glucose and lipid metabolism. Nature *414*, 799–806.

Samuel, V.T., and Shulman, G.I. (2012). Mechanisms for insulin resistance: common threads and missing links. Cell *148*, 852–871.

Streicher, J.M., Ren, S., Herschman, H., and Wang, Y. (2010). MAPK-activated protein kinase-2 in cardiac hypertrophy and cyclooxygenase-2 regulation in heart. Circ. Res. *106*, 1434–1443.

Sun, Z., Miller, R.A., Patel, R.T., Chen, J., Dhir, R., Wang, H., Zhang, D., Graham, M.J., Unterman, T.G., Shulman, G.I., et al. (2012). Hepatic Hdac3 promotes gluconeogenesis by repressing lipid synthesis and sequestration. Nat. Med. *18*, 934–942.

Tabas, I., and Ron, D. (2011). Integrating the mechanisms of apoptosis induced by endoplasmic reticulum stress. Nat. Cell Biol. *13*, 184–190.

Timmins, J.M., Ozcan, L., Seimon, T.A., Li, G., Malagelada, C., Backs, J., Backs, T., Bassel-Duby, R., Olson, E.N., Anderson, M.E., and Tabas, I. (2009). Calcium/calmodulin-dependent protein kinase II links ER stress with Fas and mitochondrial apoptosis pathways. J. Clin. Invest. *119*, 2925–2941.

Walter, P., and Ron, D. (2011). The unfolded protein response: from stress pathway to homeostatic regulation. Science *334*, 1081–1086.

Wang, Y., Vera, L., Fischer, W.H., and Montminy, M. (2009). The CREB coactivator CRTC2 links hepatic ER stress and fasting gluconeogenesis. Nature *460*, 534–537.

Wang, Y., Li, G., Goode, J., Paz, J.C., Ouyang, K., Screaton, R., Fischer, W.H., Chen, J., Tabas, I., and Montminy, M. (2012). Inositol-1,4,5-trisphosphate receptor regulates hepatic gluconeogenesis in fasting and diabetes. Nature *485*, 128–132.

Weismann, D., Erion, D.M., Ignatova-Todorava, I., Nagai, Y., Stark, R., Hsiao, J.J., Flannery, C., Birkenfeld, A.L., May, T., Kahn, M., et al. (2011). Knockdown of the gene encoding Drosophila tribbles homologue 3 (Trib3) improves insulin sensitivity through peroxisome proliferator-activated receptor-γ (PPAR-γ) activation in a rat model of insulin resistance. Diabetologia *54*, 935–944.

Wu, J., Rutkowski, D.T., Dubois, M., Swathirajan, J., Saunders, T., Wang, J., Song, B., Yau, G.D., and Kaufman, R.J. (2007). ATF6alpha optimizes long-term endoplasmic reticulum function to protect cells from chronic stress. Dev. Cell *13*, 351–364.

Yan, W., Frank, C.L., Korth, M.J., Sopher, B.L., Novoa, I., Ron, D., and Katze, M.G. (2002). Control of PERK eIF2alpha kinase activity by the endoplasmic reticulum stress-induced molecular chaperone P58IPK. Proc. Natl. Acad. Sci. USA *99*, 15920–15925.

Yang, J., MacDougall, M.L., McDowell, M.T., Xi, L., Wei, R., Zavadoski, W.J., Molloy, M.P., Baker, J.D., Kuhn, M., Cabrera, O., and Treadway, J.L. (2011). Polyomic profiling reveals significant hepatic metabolic alterations in glucagon-receptor (GCGR) knockout mice: implications on anti-glucagon therapies for diabetes. BMC Genomics *12*, 281.

Cell Metabolism, Volume *18*

Supplemental Information

Activation of Calcium/Calmodulin-Dependent Protein Kinase II in Obesity Mediates Suppression of Hepatic Insulin Signaling

Lale Ozcan, Jane Cristina de Souza, Alp Avi Harari, Johannes Backs, Eric N. Olson, and Ira Tabas

SUPPLEMENTAL INFORMATION

Activation of Calcium/Calmodulin-Dependent Protein Kinase II in Obesity Mediates Suppression of Hepatic Insulin Signaling

Lale Ozcan, Jane Cristina de Souza, Alp Avi Harari, Johannes Backs, Eric N. Olson, and Ira Tabas

Figure S1: Related to Figure 1. (A-B) Fasting plasma insulin levels and insulin tolerance tests in DIO *Camk2g*$^{-/-}$ (n=7) or WT (n=10) mice (mean ± SEM; ** p<0.01). (C) Representative images of H&E staining of liver sections from the two groups of mice. Scale bar, 20 μm. For quantification, 2 separate liver sections from 5 mice in each group were analyzed for the percentage of HCs containing lipid droplets greater than 2 μm in diameter (mean ± SEM; ** p<0.01).

Figure S2: Related to Figure 3. (A) *Ob/ob* mice administered adeno-LacZ or -K43A-CaMKII were fasted for 6 h and then injected with 2 IU/kg insulin through the portal vein. Liver extracts were assayed for p-Akt, total Akt, and β-actin by immunoblot or immunoprecipitated for IRS-1 or IR and then assayed by immunoblot for IRS-1, IR, or phospho-Tyr (PY). Densitometric quantification of the immunoblot data is shown in the graph (mean ± SEM; *p < 0.05). (B) As in (A), except WT lean mice were used. (C) As in (A), except adeno-T222A-MK2 was used (mean ± SEM; *p < 0.05).

Figure S3: Related to Figures 3-4. Improvement in Insulin-induced Akt Phosphorylation in *Camk2g*$^{-/-}$ Hepatocytes is not Abrogated by Restoring Nuclear FoxO1. (A-B) HCs from *Camk2g*$^{fl/fl}$ mice were transduced with adeno-LacZ or -Cre, and then 4 h later half of the adeno-Cre-transduced cells received HA-tagged adeno-FoxO1-ADA while the other half received adeno-LacZ control. After an additional 24 h of incubation, the cells were incubated with palmitate and then insulin as in Figure 4. One set of cells were harvested and assayed for *Igfbp1* mRNA levels by RT-qPCR (A), and another set was assayed for p-Akt, total Akt, β-actin by immunoblotting and then quantified by densitometry (B). Data are mean ± SEM; bars with different symbols are different from each other and from control, p< 0.005. (C) Nuclear FoxO1 and nucleophosmin (Np) were probed by immunoblot in livers from *ob/ob* mice treated with adeno-LacZ or -K43A-CaMKII. Densitometric quantification of the immunoblot data is shown in the graph (mean ± SEM; *p < 0.05). (D) Sixteen-week-old DIO mice were administered adeno-LacZ or K43A-CaMKII, and then, two days later, half of the adeno-K43A-CaMKII mice received adeno-FoxO1-ADA, while the other half received adeno-LacZ control. Three weeks later, mice were fasted for 6 h and then injected with 1.5 IU/kg insulin through the portal vein. Liver extracts were assayed for p-Akt, total Akt, β-actin or nuclear FoxO1 and nucleophosmin (Np) by immunoblot.

Figure S4: Related to Figure 5. (A) HCs from *Camk2g*$^{fl/fl}$ mice were transduced with adeno-LacZ or -Cre and then 24 h later incubated with BSA or palmitate (0.2 mM) for 19 h. *Trb3* mRNA levels were analyzed by RT-qPCR (mean ± SEM; different symbols indicate $p< 0.05$). (B) DIO *Camk2g*$^{fl/fl}$ mice were treated with TBG-Cre or TBG-LacZ, and one week later half of the TBG-LacZ mice received adeno-TRB3, while the other half received adeno-LacZ control. Eight days later, after 6 h fasting, the mice were injected with 1.5 IU/kg insulin through the portal vein. Total liver extracts were assayed for p-Akt, total Akt, TRB3, and β-actin by immunoblot. Densitometric quantification of the immunoblot data are shown in the graph (mean ± SEM; bars with different symbols are different from each other and from control, $p < 0.05$). (C) HCs from *Camk2g*$^{fl/fl}$ mice were transduced with adeno-LacZ or -Cre and five hours later, half of the adeno-LacZ treated cells received adeno-shTRB3, while the other half received adeno-LacZ control. 24 h later, the cells were incubated with either BSA control or palmitate (0.2 mM) for 19 h, with the last 5 h in serum-free media followed by ± 100 nM insulin stimulation for 5 min. One set of cells were harvested and assayed for p-Akt, total Akt, β-actin by immunoblotting and another set was assayed for *Trb3* mRNA levels by RT-qPCR (mean ± SEM; bars with different symbols are different from each other and from control, $p< 0.05$). (D) As in (B) except nuclear FoxO1 and nucleophosmin (Np) were probed by immunoblot in livers from DIO mice treated with LacZ or K43A-CaMKII. Densitometric quantification of the immunoblot data is shown in the graph (mean ± SEM; *$p < 0.05$). (E) HCs from *Camk2g*$^{fl/fl}$ mice were transduced with adenoviral vectors expressing LacZ or Cre and 4 h later, half of the adeno-Cre treated cells received TRB3 whereas the rest received LacZ. 24 h later, cells were serum-depleted overnight and then incubated for 5 h with forskolin (10 μm) in serum-free media. RNA was assayed for *G6Pc*, *Pck1* and *Trb3* mRNA (mean ± SEM; *$p < 0.05$).

Figure S5: Related to Figure 6. Deficiency of p38α or CaMKII Suppresses the PERK Branch of the UPR. (A-B) HCs from *Camk2g*$^{fl/fl}$ mice were transduced with adenoviral vectors expressing LacZ or Cre at an MOI of 10. After 24 h, cells were incubated with tunicamycin (0.5 μg/ml) for 4 h or with palmitate (0.2 mm) for 19 h. Lysates were immunoblotted for p-PERK, PERK, CHOP and β-actin by immunoblot. (C) As in (A) except that *Mapk14*$^{fl/fl}$ HCs were used. (D) *Chop* mRNA levels were assayed by RT-qPCR in the livers of *ob/ob* mice treated with adeno-LacZ or -K43-CaMKII or in the livers of DIO WT or *Camk2g*$^{-/-}$ mice (mean ± SEM; *$p < 0.05$). (E) HCs from

Camk2g$^{fl/fl}$ mice were treated as in (B). RNA was extracted and assayed for spliced and unspliced *Xbp1* and *Gapdh* loading control by RT-PCR. Tunicamycin (0.5 μg/ml) treated HCs were used as a positive control. (F) Livers from *ob/ob* mice treated with adeno-LacZ or -K43A-CaMKII were assayed for spliced and unspliced *Xbp1* and *Gapdh* loading control by RT-PCR. Tunicamycin (0.5 μg/ml) treated HCs were used as a positive control.

Figure S6: Related to Figure 7. Deficiency of CaMKII or P38α Increases *p58*^{ipk} and Nuclear ATF6. (A) HCs from *Camk2g*$^{fl/fl}$ mice were transduced with adeno-LacZ or -Cre. After 24 h, *p58*^{ipk} mRNA levels were assayed by RT-qPCR (mean ± SEM; * $p < 0.05$). (B) HCs from *Mapk14*$^{fl/fl}$ mice were transduced with adenoviral vectors expressing LacZ or Cre at an MOI of 10. After 24 h, the cells were incubated with tunicamycin (0.5 μg/ml) for 5 h and *p58*^{ipk} mRNA levels were assayed (mean ± SEM; bars with different symbols are different from each other and control, $p < 0.05$). (C) *p58*^{ipk} mRNA levels were assayed in livers of DIO *Camk2g*$^{fl/fl}$ mice treated with AAV-TBG-Cre or AAV-TBG-LacZ (mean ± SEM; *$p < 0.05$). (D) HCs from WT mice were transduced with adeno-LacZ or -K43A-CaMKII. After 24 h, the cells were treated with tunicamycin for the indicated times. Nuclear extracts were immunoblotted for ATF6 and nucleophosmin (Np) as a loading control.

Supplemental Experimental Procedures

Reagents and Antibodies

Sodium palmitate, tunicamycin, and insulin were from Sigma. Anti-ATF-4, anti-CHOP, anti-phosphotyrosine, and anti-IR antibodies were from Santa Cruz Biotechnology, Inc. Anti-β-actin and anti-$p58^{IPK}$ were from Abcam. Anti-phospho-S473-Akt, anti-phospho-T308-Akt, anti-Akt, anti-IRS2, anti-nucleophosmin (Np), anti-FoxO1, anti-phospho-S253-FoxO1, anti-phospho-S9-GSK3β, anti-GSK3β, anti-HA, anti-phospho-PERK, and anti-PERK antibodies were from Cell Signaling. Anti-ATF6 antibody was from Imgenex. Adenoviruses encoding LacZ, T287D-CaMKII, and K43A-CaMKII were gifts from Dr. Harold A. Singer (Albany Medical College); TRB3 and TRB3 RNAi adenoviruses were gifts from Dr. Marc Montminy (Salk Institute for Biological Studies), adeno-ATF-4 was a gift from Randal J. Kaufman (Sanford-Burnham Medical Research Institute), and adeno-FoxO1-ADA was a gift from Dr. Domenico Accili (Columbia University). All adenoviruses were amplified by Viraquest, Inc. Adeno-associated viruses (AAV) containing either hepatocyte-specific TBG-Cre recombinase (AAV8-TBG-Cre) or the control vector (AAV8-TBG-LacZ) were purchased from the Penn Vector Core. Adeno-T222A-MK2 was purchased from Cell Biolabs Inc.

Immunoprecipitation

Cell lysate from tissues (~1 mg total protein) or cells (~350 μg total protein) were brought to a total volume of 1 ml with lysis buffer. Antibodies (0.3-0.6 μg) and protein A Sepharose beads (80 μl) were added to the tube, which was then rotated at 4°C overnight. Immune complexes were collected by centrifugation at 16,000 x g and washed 3 times with chilled lysis buffer.

Immunoblot and RT-qPCR Assays

Immunoblot and RT-qPCR assays were performed as previously described (Timmins et al., 2009). Total RNA was extracted from HCs using the RNeasy kit (Qiagen). cDNA was synthesized from 1 μg total RNA using oligo (dT) and Superscript II (Invitrogen). Nuclear extraction from liver was performed using the Nuclear Extraction Kit from Panomics according to the manufacturer's instructions.

XBP1 splicing

Total RNA was reverse-transcribed into cDNA. A segment of XBP-1 mRNA was amplified using the forward primer AAC TCC AGC TAG AAA ATC AGC and the reverse primer ACC ACC ATG GAG AAG GCT GG. Spliced and unspliced XBP-1 were resolved by electrophoresis in a 2.5% agarose gel and visualized using ethidium bromide under UV light. GAPDH, using CCA TGG GAA GAT GTT CTG GG and CTC AGT GTA GCC CAG GAT GC as forward and reverse primers, respectively, was used as an internal standard to verify equal RT product loading for each experiment.

Liver Triglyceride Measurement

Lipid extraction was performed using a modification of the Bligh-Dyer method (Bligh and Dyer, 1959). Briefly, livers were homogenized in chloroform: MeOH: H2O (1:2:0.8) at room temperature and then centrifuged. Equal volumes of chloroform and water were added to the supernatant fraction, which was then vortexed and centrifuged. The chloroform layer was collected and dried under nitrogen. The dried lipids were then resuspended in 90% isopropanol: 10% Triton-X and then assayed for triglyceride using a kit from Wako and cholesterol using a kit from Life Technologies.

Glucose Production in Primary HCs

After primary mouse HCs were harvested and cultured as described above, the cell culture medium was switched to glucose- and phenol-free DMEM (pH 7.4) supplemented with 20 mM sodium lactate and 2 mM sodium pyruvate. After 20 h of culture, 500 ml medium was collected, and the glucose content was measured using a colorimetric glucose assay kit (Abcam). The readings were then normalized to the total protein amount in the whole-cell lysates.

REFERENCES

Bligh, E.G., and Dyer, W.J. (1959). A rapid method of total lipid extraction and purification. Can. J. Biochem. Physiol. *37*, 911-917.

Timmins, J.M., Ozcan, L., Seimon, T.A., Li, G., Malagelada, C., Backs, J., Backs, T., Bassel-Duby, R., Olson, E.N., Anderson, M.E., and Tabas, I. (2009). Calcium/calmodulin-dependent protein kinase II links ER stress with Fas and mitochondrial apoptosis pathways. J. Clin. Invest. *119*, 2925-2941.

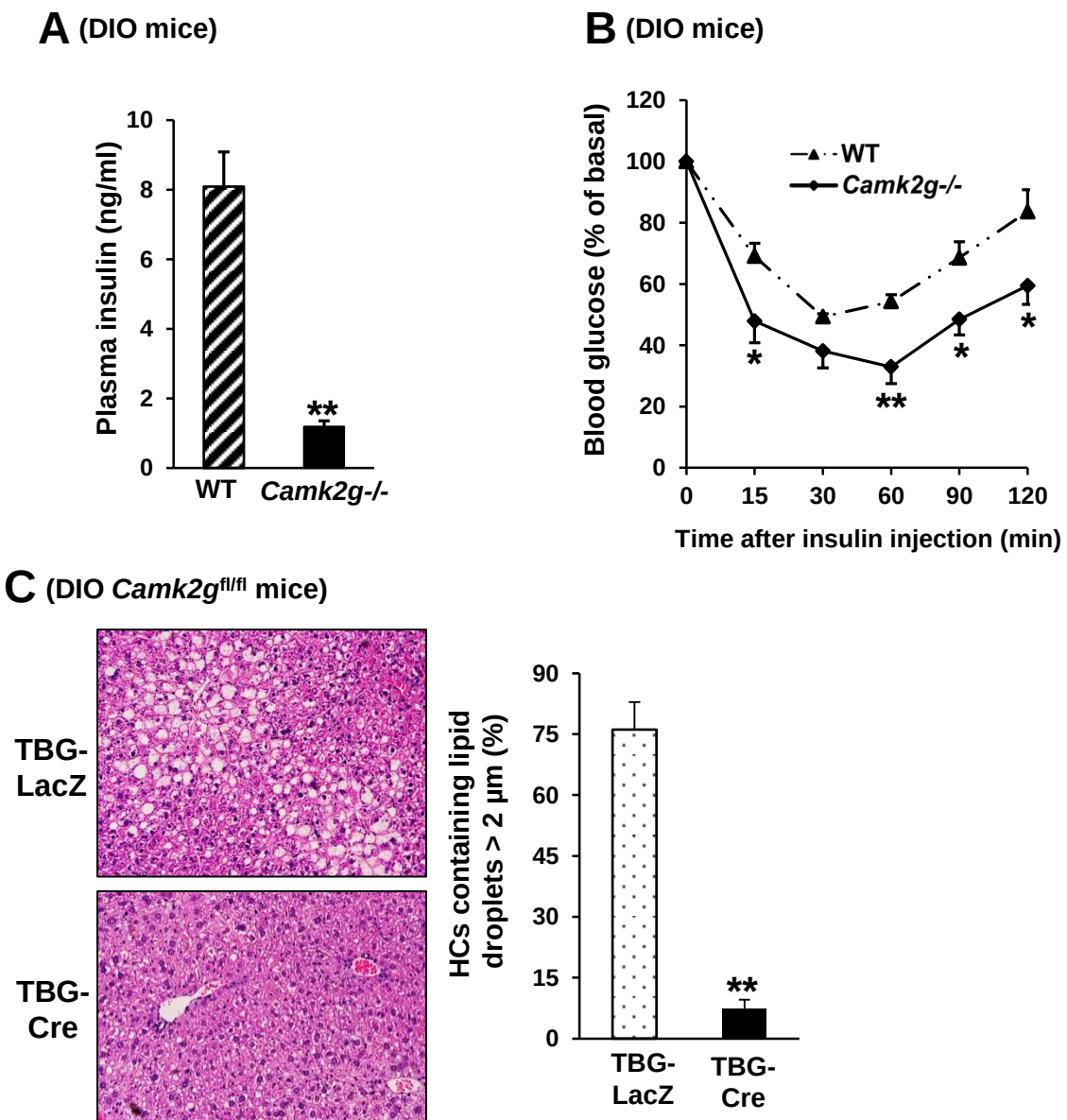
A (DIO mice)
Plasma insulin (ng/ml)
10
8
6
4
2
0
**
WT
Camk2g-/-
B (DIO mice)
Blood glucose (% of basal)
120
100
80
60
40
20
0
WT
Camk2g-/-
*
**
*
*
0
15
30
60
90
120
Time after insulin injection (min)
C (DIO Camk2g fl/fl mice)
TBG-LacZ
TBG-Cre
HCs containing lipid droplets > 2 µm (%)
90
75
60
45
30
15
0
**
TBG-LacZ
TBG-Cre

A (livers from *ob/ob* mice)

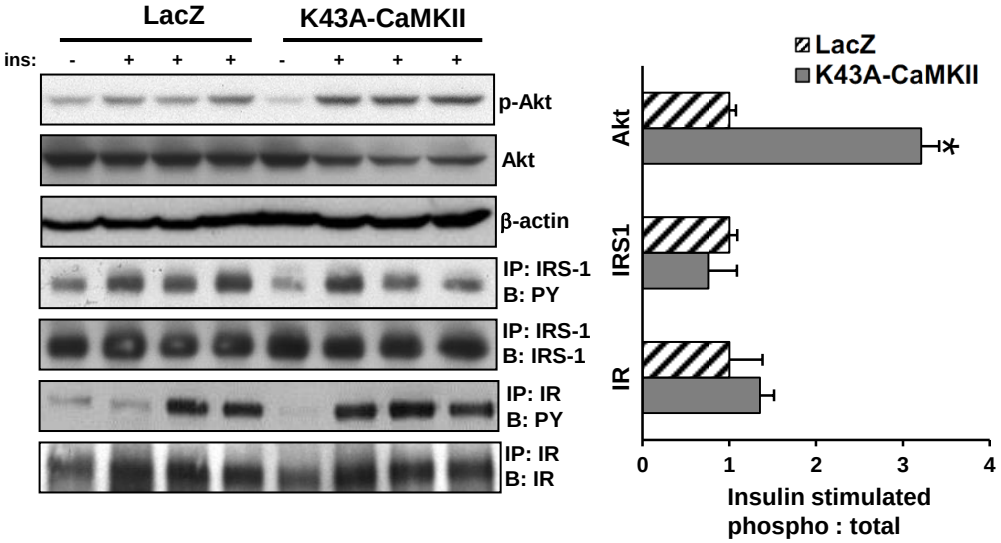

C (livers from *ob/ob* mice)

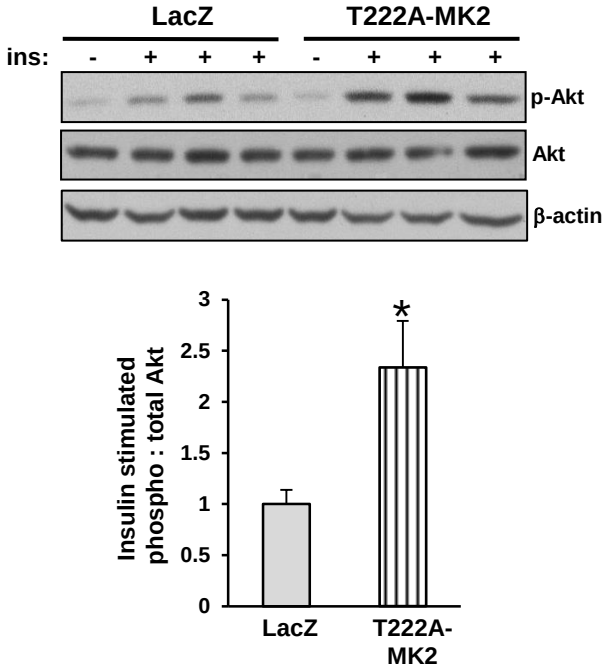

B (livers from lean mice)

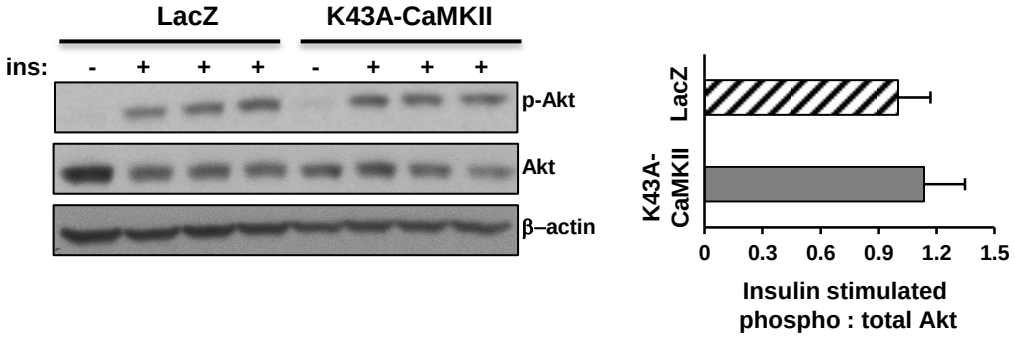

Figure S3

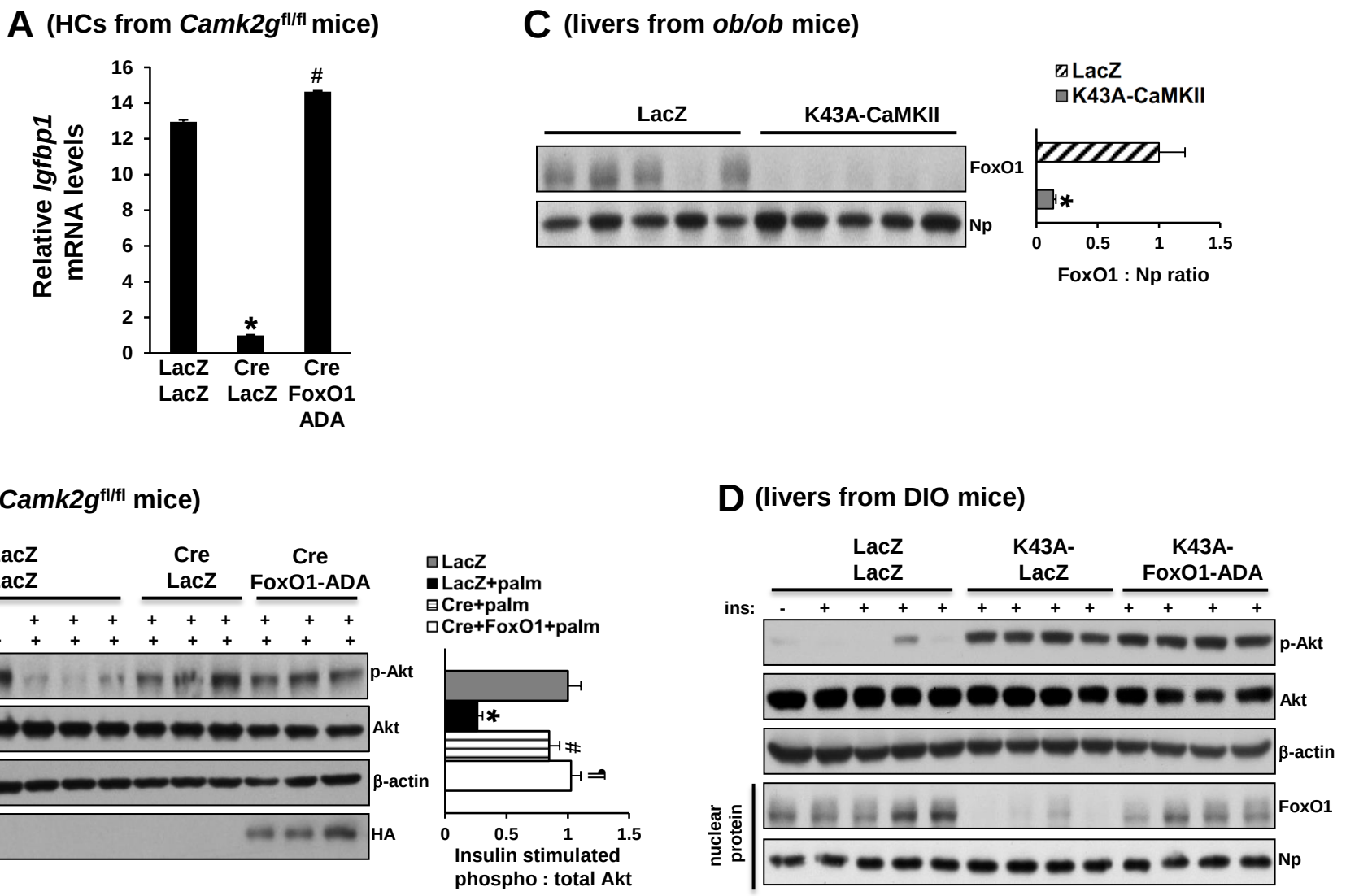
A (HCs from Camk2g fl/fl mice)
Relative Igfbp1 mRNA levels
16
14
12
10
8
6
4
2
0
*
#
LacZ LacZ
Cre LacZ
Cre FoxO1 ADA
C (livers from ob/ob mice)
LacZ
K43A-CaMKII
FoxO1
Np
LacZ
K43A-CaMKII
*
0
0.5
1
1.5
FoxO1 : Np ratio
B (HCs from Camk2g fl/fl mice)
LacZ LacZ
Cre LacZ
Cre FoxO1-ADA
palm:
ins:
p-Akt
Akt
β-actin
HA
LacZ
LacZ+palm
Cre+palm
Cre+FoxO1+palm
*
#
0
0.5
1
1.5
Insulin stimulated phospho : total Akt
D (livers from DIO mice)
LacZ LacZ
K43A-LacZ
K43A-FoxO1-ADA
ins:
p-Akt
Akt
β-actin
nuclear protein
FoxO1
Np

Figure S4

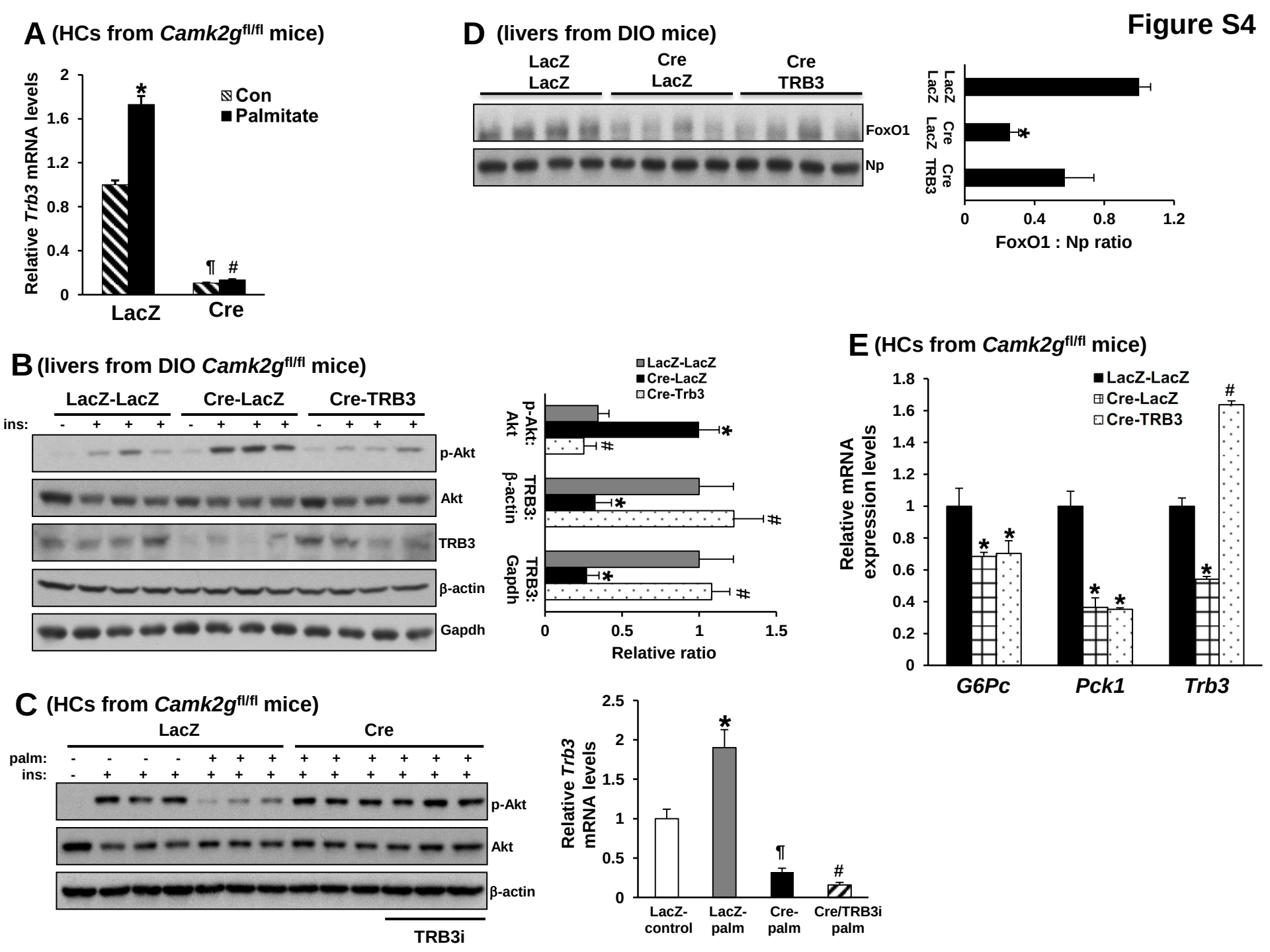
A (HCs from Camk2g fl/fl mice)
Relative Trb3 mRNA levels
Con
Palmitate
LacZ
Cre
B (livers from DIO Camk2g fl/fl mice)
LacZ-LacZ
Cre-LacZ
Cre-TRB3
ins:
p-Akt
Akt
TRB3
β-actin
Gapdh
LacZ-LacZ
Cre-LacZ
Cre-Trb3
p-Akt: Akt
TRB3: β-actin
TRB3: Gapdh
Relative ratio
C (HCs from Camk2g fl/fl mice)
LacZ
Cre
palm:
ins:
p-Akt
Akt
β-actin
TRB3i
Relative Trb3 mRNA levels
LacZ-control
LacZ-palm
Cre-palm
Cre/TRB3i palm
D (livers from DIO mice)
LacZ LacZ
Cre LacZ
Cre TRB3
FoxO1
Np
FoxO1 : Np ratio
E (HCs from Camk2g fl/fl mice)
LacZ-LacZ
Cre-LacZ
Cre-TRB3
Relative mRNA expression levels
G6Pc
Pck1
Trb3

Figure S5

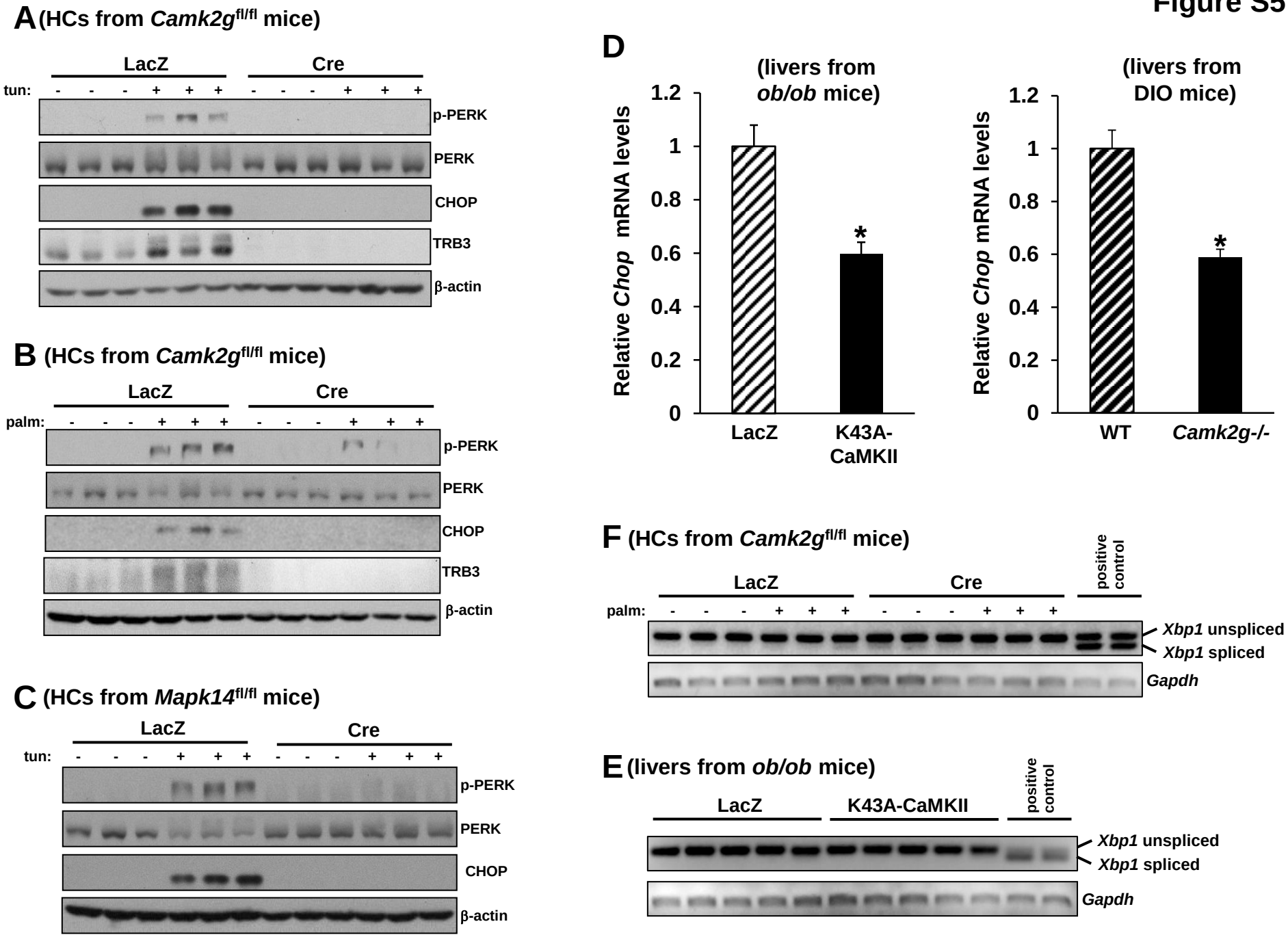
A (HCs from Camk2g fl/fl mice)
LacZ
Cre
tun: - - - + + + - - - + + +
p-PERK
PERK
CHOP
TRB3
β-actin
B (HCs from Camk2g fl/fl mice)
LacZ
Cre
palm: - - - + + + - - - + + +
p-PERK
PERK
CHOP
TRB3
β-actin
C (HCs from Mapk14 fl/fl mice)
LacZ
Cre
tun: - - - + + + - - - + + +
p-PERK
PERK
CHOP
β-actin
D
(livers from ob/ob mice)
Relative Chop mRNA levels
1.2
1
0.8
0.6
0.4
0.2
0
*
LacZ
K43A-CaMKII
(livers from DIO mice)
Relative Chop mRNA levels
1.2
1
0.8
0.6
0.4
0.2
0
*
WT
Camk2g-/-
F (HCs from Camk2g fl/fl mice)
LacZ
Cre
positive control
palm: - - - + + + - - - + + +
Xbp1 unspliced
Xbp1 spliced
Gapdh
E (livers from ob/ob mice)
LacZ
K43A-CaMKII
positive control
Xbp1 unspliced
Xbp1 spliced
Gapdh

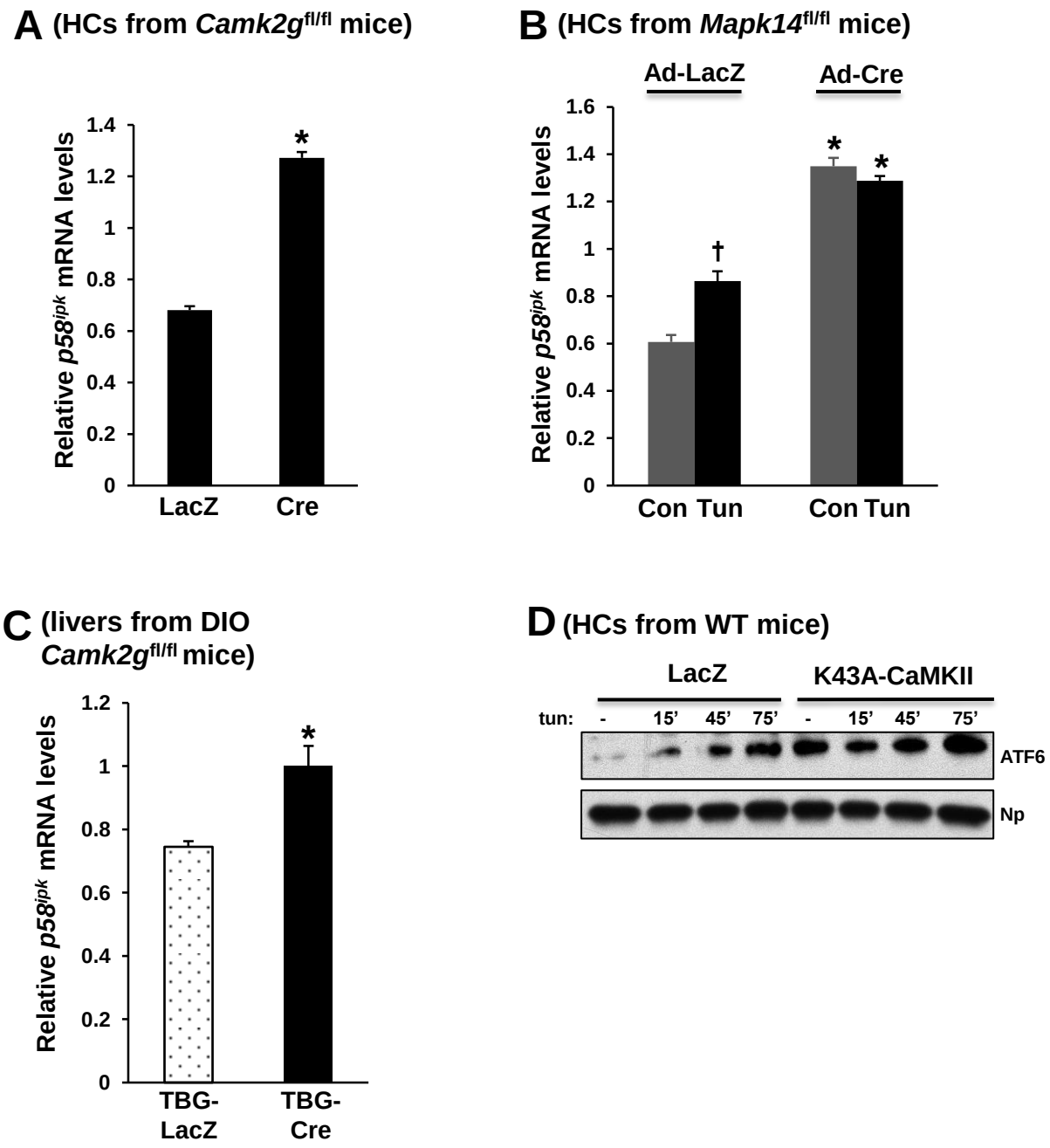
A (HCs from Camk2g fl/fl mice)
Relative p58ipk mRNA levels
1.4
1.2
1
0.8
0.6
0.4
0.2
0
*
LacZ
Cre
B (HCs from Mapk14 fl/fl mice)
Ad-LacZ
Ad-Cre
Relative p58ipk mRNA levels
1.6
1.4
1.2
1
0.8
0.6
0.4
0.2
0
†
*
*
Con Tun
Con Tun
C (livers from DIO Camk2g fl/fl mice)
Relative p58ipk mRNA levels
1.2
1
0.8
0.6
0.4
0.2
0
*
TBG-LacZ
TBG-Cre
D (HCs from WT mice)
LacZ
K43A-CaMKII
tun:
-
15'
45'
75'
-
15'
45'
75'
ATF6
Np